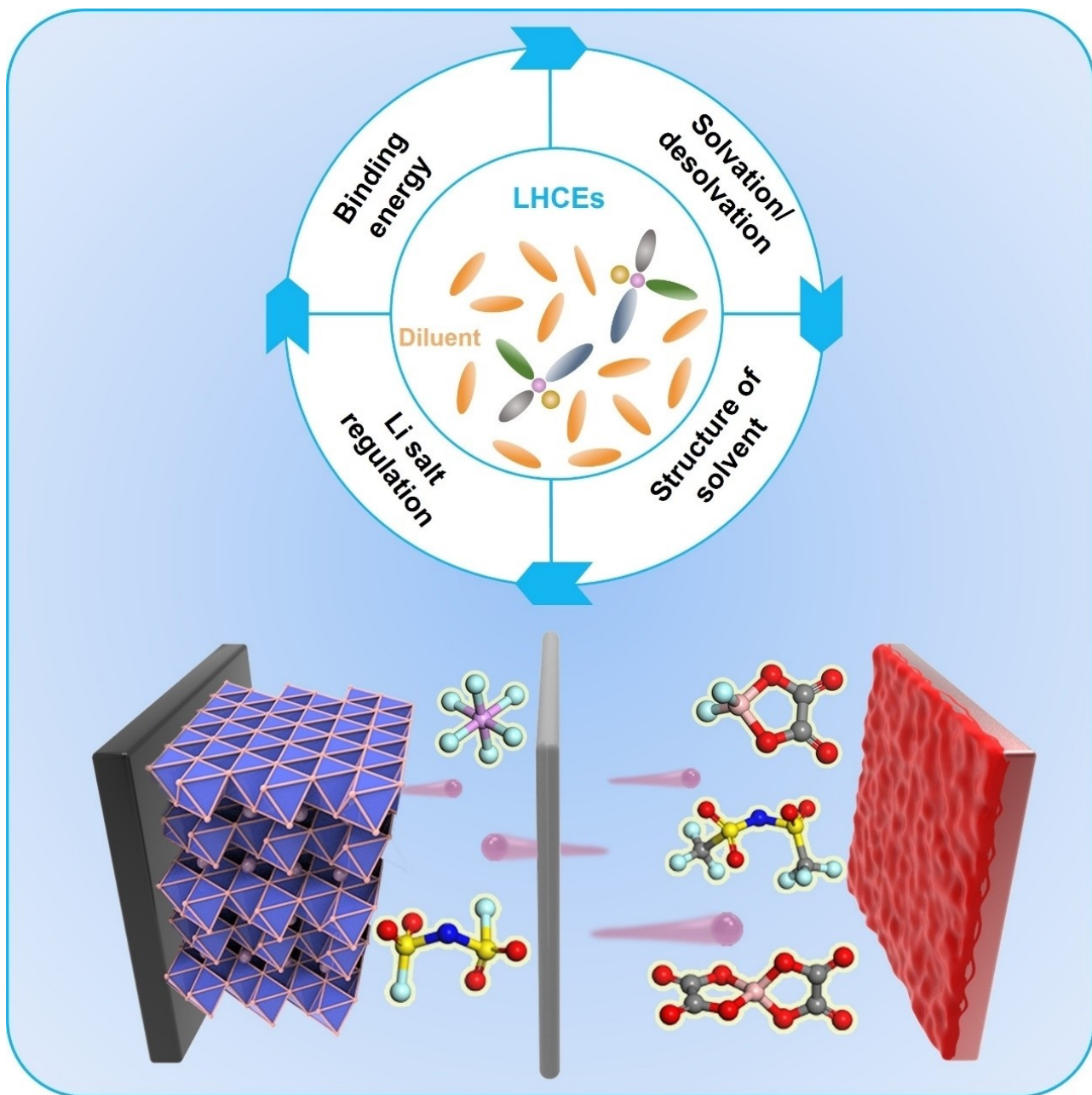


VIP Very Important Paper

www.batteries-supercaps.org

# Constructing Low-Solvation Electrolytes for Next-Generation Lithium-Ion Batteries

Jipeng Liu,<sup>[a, b, c]</sup> Botao Yuan,<sup>[a]</sup> Liwei Dong,<sup>[b]</sup> Shijie Zhong,<sup>[a]</sup> Yuanpeng Ji,<sup>[b]</sup> Yuanpeng Liu,<sup>[a]</sup> Jiecai Han,<sup>[a]</sup> Chunhui Yang,<sup>[b, c]</sup> and Weidong He<sup>\*[a, d, e]</sup>



The realization of high-concentration electrolytes (HCEs) is a benchmark breakthrough attributed to the modification of cation aggregation, which owns technical advantages over the widely used conventional electrolytes. Due to the high cost brought by the large amount of lithium (Li) salts, high viscosity, low Li<sup>+</sup> conductivity, and wettability of the HCE system, the concept of localized HCEs (LHCEs) is proposed to improve the aforementioned shortcomings without affecting the performances of high-energy-density batteries. Nevertheless, the effect factors of the weakly solvated structure of LHCEs have not been summarized, so it is urgent to conclude this direction to further survey the low-solvation structure and properties. Hence, for

the first time we offer a comprehensive and distinct overview on the electrolyte development, strategies for constructing low-solvation structure, and scientific perspectives for lithium-ion batteries, especially by focusing on the binding energies between cation and solvents, solvation and de-solvation process, structure of novel solvents, and selection of Li salts. Emphasis is placed on the relevance of constructing low-solvation structure and forming electrode/electrolyte interphases, and new insights into weakly solvated electrolytes associated with efficient solid electrolyte interphase and cathode electrolyte interphase layers are presented for developing next-generation lithium-ion batteries.

## 1. Introduction

The electrolyte is aptly described as “blood” in rechargeable lithium-ion batteries (LIBs), which interacts closely with other components in electrochemical energy storage and conversion devices. It makes an irrefutable contribution to facilitating fast Li<sup>+</sup> transport between cathode and anode, and preventing the electrode/electrolyte interphases from severe damage to the electrode, enabling LIBs to work in stable chemical environments and high operating voltages conditions.<sup>[1]</sup>

Although the solvation structure is important in both Li-ion and Li-metal batteries, its role remains controversial. In particular, the development of solvated structural models has been slow since the introduction of ion-solvent interactions from the Debye-Hückel theory in 1973, as shown in Figure 1(a).<sup>[2]</sup> The “ionic solvation coordination” model reported in 1974 is the latest model that can be extended from aqueous electrolytes to non-aqueous electrolytes and to binary solvent solutions with solvent-competing coordination. Dr. M Stanley Whittingham pioneered the development of the first rechargeable battery in the 1970s and won the Nobel Prize in 2019, heralding the arrival of a new energy era.<sup>[3]</sup> Dahn was a pioneer in battery electrolyte development. In 1990, Dahn designed an ethylene carbonate (EC) solvent to resolve the co-intercalation problem of propylene carbonate (PC) solvent by repairing the graphite/electrolyte interphase,<sup>[4]</sup> and this critical progress led

to the application of carbonate-based electrolytes until 2010.<sup>[5]</sup> However, when the aggressive voltage cathode and low voltage anode of high energy density batteries are matched, the conventional electrolytes with low Li salt concentration cannot meet the exorbitant working potential.<sup>[6]</sup> Therefore, notable efforts have been centered on developing advanced electrolytes, among which high-concentration electrolytes (HCEs) have received extensive attention due to their excellent compatibility with mainstream electrodes, wide voltage windows, and high safety.<sup>[1b,7]</sup> The lithium salt concentration of HCEs usually >3 M, and it exhibits various physical and chemical properties compared to conventional electrolytes due to their unique solvation structure. In HCEs, the interaction between cations and anions is stronger, and there are almost no free solvent molecules, which reduces the decomposition of the solvent in the solid electrolyte interphase (SEI) and cathode electrolyte interphase (CEI), resulting in higher cycling stability and Coulombic efficiency (CE). However, due to the high cost of abundant Li salts, high viscosity, low Li<sup>+</sup> conductivity, and inferior wettability of the HCEs system, the practical production, and application of the HCEs system are hindered.

Following HCEs, Pacific Northwest National Laboratory proposed the concept of localized HCEs (LHCEs), which improves the aforementioned shortcomings without affecting the performance of high-energy-density batteries.<sup>[8]</sup> The key feature of LHCEs compared to conventional dilute electrolytes and HCEs is their unique solvation structure: high concentrations of salt-solvent clusters distributed in non-solvating solvent (diluent) molecules. The lowest unoccupied molecular orbital (LUMO) shifts from the solvent to the anion as the solvated structure shifts from solvent-separated ion pairs (SSIPs) in conventional electrolytes to contact ion pairs (CIPs) in HCEs and aggregated LHCEs. Further studies on the potential mechanism for the improved performances of LHCEs than in the corresponding HCEs reveal that the diluent molecules around the high-concentration clusters jointly participate in the formation of the electrolyte/electrode interphase, further improving the performances of the interphase. However, the origin of the weakly solvated structure of LHCEs has not been comprehensively summarized, so it is urgent to conclude this direction to improve its structure and properties.

[a] Dr. J. Liu, Dr. B. Yuan, Dr. S. Zhong, Assoc. Prof. Y. Liu, Prof. J. Han, Prof. W. He  
 National Key Laboratory of Science and Technology on Advanced Composites in Special Environments, and Center for Composite Materials and Structures, Harbin Institute of Technology, Harbin 150080, China  
 E-mail: weidong.he@hit.edu.cn

[b] Dr. J. Liu, Dr. L. Dong, Dr. Y. Ji, Prof. C. Yang  
 MIIT Key Laboratory of Critical Materials Technology for New Energy Conversion and Storage, School of Chemistry and Chemical Engineering, Harbin Institute of Technology, Harbin 150001, China

[c] Dr. J. Liu, Prof. C. Yang  
 State Key Laboratory of Urban Water Resource and Environment, Harbin Institute of Technology, Harbin 150001, China

[d] Prof. W. He  
 Chongqing Research Institute, Harbin Institute of Technology, Chongqing 401151, China

[e] Prof. W. He  
 School of Mechanical Engineering, Chengdu University, Chengdu 610106, China

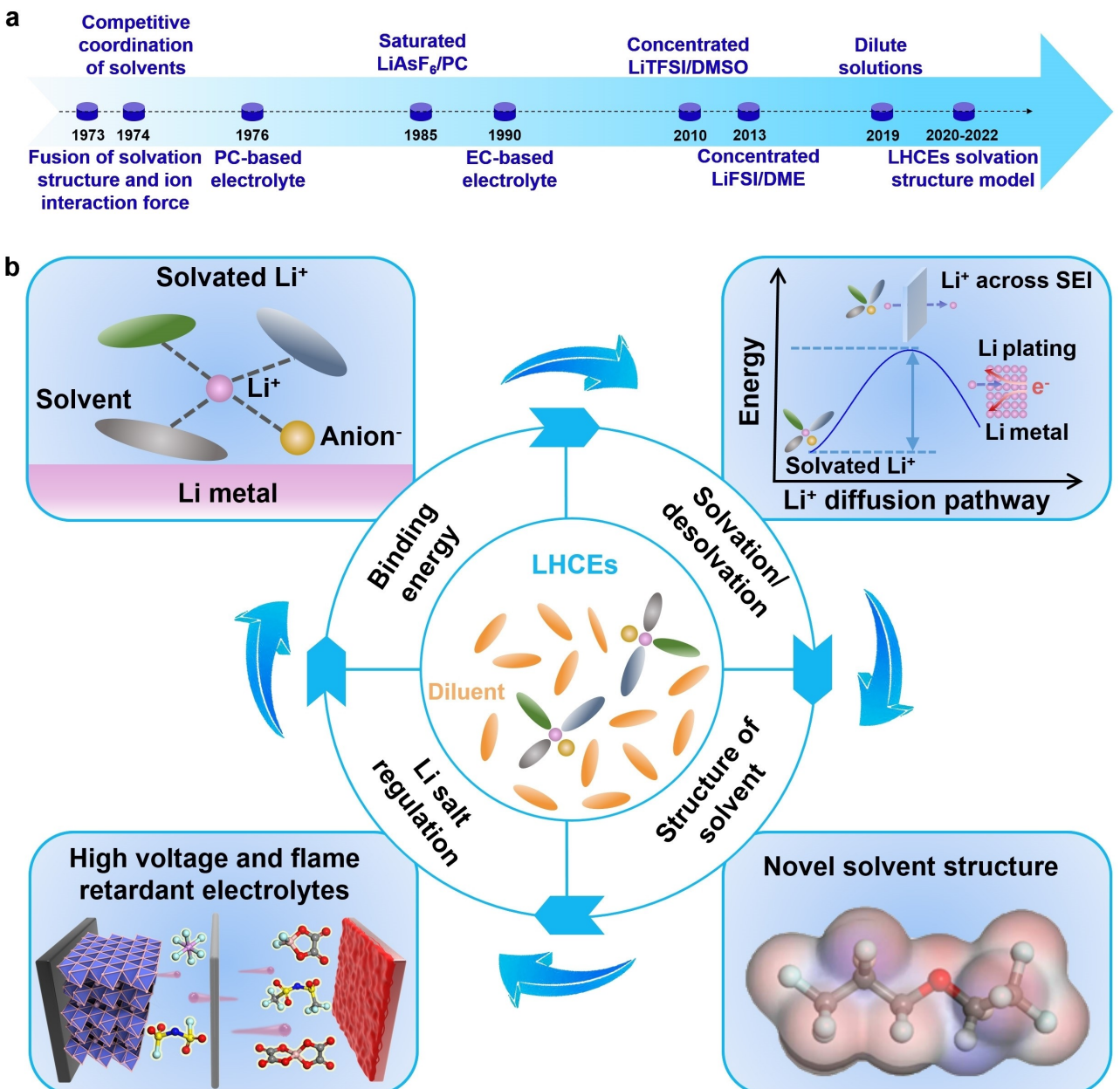


**Figure 1.** a) Timeline of the solvation theory and LHCEs system.<sup>[7-24]</sup> b) Overview of the factors of low-solvation structure including the binding energy, activation energy, solvation/de-solvation process, structure of novel solvents, and selection of Li salts. Reproduced with permission from Ref. [1e]. Copyright (2021) WILEY-VCH.



Jipeng Liu is a PhD student in the Center for Composite Materials and Structures, Harbin Institute of Technology, and researching electrodes and electrolytes for lithium-ion batteries. His research involves the design of electrolytes and electrodes for special environment lithium ion batteries and the synthesis of advanced energy materials for lithium based batteries.



Weidong He is a professor at Harbin Institute of Technology, leading a group of researchers working on synthesis, property analysis, and theoretical simulations of energy materials for batteries and fuel cells. He received his Ph.D. from Vanderbilt University in 2012. He then went to Pacific Northwest National Laboratory for his postdoctoral research. His research involves designing efficient battery/fuel cell systems with pre-evaluated electrodes, electrolytes, and operating conditions.

When integrating the solvation coordination structure of LHCEs, we propose to pay extensive attention to the following branches in Figure 1(b). First, the binding energy of cation and solvent depends on the electrostatic force between the oxygen atom of the solvent molecule and  $\text{Li}^+$ .<sup>[9]</sup> Second, during the high-rate charge-discharge process, the activation energy and the solvation/de-solvation process will regulate the kinetic behavior.<sup>[10]</sup> Thus, how to reduce the activation energy and work out the process and location of the solvation/de-solvation process are two problems that need to be solved urgently in the future,<sup>[11]</sup> which are rarely studied in the previous literature. Third, the diverse structure of solvent molecules is significant.<sup>[12]</sup> Although the molecular formula of the solvent is the same, the cyclic and chained molecules own different binding energies to  $\text{Li}^+$ . Both the symmetrical nature of the solvation group between the molecule and the cation and the functional groups of the ring/chain solvent can affect the stacking form of the molecule. Fourth, the shell of low-solvation structure also derives from various anions of Li salts.<sup>[1b,13]</sup> Among them, the coordination ratio of solvent molecules to cations gradually decreases with the increase of anion concentration in the solution. Once the solvent molecules around the cation are sufficient to participate in the formation of the primary solvation shell, the anion is found in the primary solvation shell. It is reduced/oxidized as the voltage decreases/increases, resulting in different electrode/electrolyte interphases. Limited by *in situ* nano-characterization techniques and research methods, the research progress on the solvation structure of electrolytes is slow.<sup>[8d,14]</sup> Therefore, finding factors in constructing the solvation structure of electrolytes, exploring the de-solvation behavior of  $\text{Li}^+$ , and contriving advanced characterization techniques are expected to break through the bottleneck of the solvation structure of electrolytes to improve electrode/electrolyte interphases.<sup>[15]</sup>

## 2. Binding Energy Constructing Low-Solvation Structure

The understanding of interfaces is still in its infancy due to the limitations of research techniques and the changes in interface properties with time and potential.<sup>[16]</sup> An important consideration in constructing the electrode/electrolyte interphases is the solvated coordination structure of the bulk solution,<sup>[17]</sup> which has been widely described and accepted over the past few years. The binding energy between electrolyte components largely determines the  $\text{Li}^+$  solvation structure,  $\text{Li}^+$  diffusion properties, electrolyte stability, and electrolyte-electrode interface properties.<sup>[18]</sup> For example, the coordination with solvent molecules and anions determines the solvated structure of  $\text{Li}^+$ , which further regulates the migration, de-solvation, and nucleation of  $\text{Li}^+$ . The interaction with  $\text{Li}^+$  also changes the redox stability of solvent molecules and anions, further regulating the formation of SEI and CEI.<sup>[19]</sup> Most significantly, the evolution of the electrode/electrolyte interphases acts a crucial role in enhancing the electrochemical property and

extending the lifetime to satisfy the sustainable energy demands of a mobile society.<sup>[20]</sup> Therefore, the binding energy between the electrolytes directly determines the properties of the bulk electrolyte and the interfacial electrolyte, thereby determining the performances of the battery. Understanding the complex interaction and interrelationship between them and electrolyte properties is of great significance for exploring the working mechanism of lithium battery electrolytes and enabling rational design beyond traditional trial-and-error methods. We summarize the latest research progress on binding energies between  $\text{Li}^+$  and solvents constructing solid electrolyte interphase (SEI) and cathode electrolyte interphase (CEI) in rechargeable LIBs systems.

### 2.1. SEI derived from binding energy

In recent decades, researchers have centered on solving the uncontrollable growth of Li dendrites.<sup>[21]</sup> The commonly used method blocks Li dendrites physically with separators or consumes Li dendrites through chemical redox reactions to build solid artificial SEI from nano/micro scales.<sup>[22]</sup> The SEI can regulate the uniform deposition of  $\text{Li}^+$ , and various three-dimensional current collectors are applied as host materials to tune the exfoliation and deposition processes of Li metal,<sup>[23]</sup> which are usually inconvenient, expensive, and hard to provide in large quantities.

At present, the practical and straightforward method is directly adding additives to the commercial electrolyte by constructing various solvation structure of  $\text{Li}^+$ , further forming a more stable and smoother SEI layer. Therefore, by adjusting the binding energies between  $\text{Li}^+$  and solvents, the solvent shell of  $\text{Li}^+$  can be changed, thereby improving the SEI composition during the  $\text{Li}^+$  reduction process. Liao et al. at the Chinese University of Science and Technology creatively used  $\text{RbNO}_3$  as an electrolyte additive.<sup>[29]</sup> Specifically, the low concentration of rubidium ions ( $\text{Rb}^+$ ) has a lower reduction potential than that of  $\text{Li}^+$  and participate in forming the weak solvation sheath of  $\text{Li}^+$ , which generates a highly conductive SEI layer containing  $\text{LiN}_x\text{O}_y$  and  $\text{Li}_3\text{N}$ . The additive can regulate the deposited morphology of  $\text{Li}^+$  and further avoid the formation of Li dendrites.

Sun et al. investigated an inexpensive and straightforward succinic anhydride (SA) molecule to improve the CE of Li plating and stripping in Figures 2(a and b).<sup>[24]</sup> The strong binding energy of  $\text{Li}^+$  with SA molecule ( $-0.77$  eV) changes the solvated structure of  $\text{Li}^+$  and increases the deposition energy barrier of  $\text{Li}^+$ , resulting in a higher overpotential for Li electrodeposition. The increase of overpotential favors the formation of more nucleation sites, reducing the size of Li nuclei and forming a smooth Li deposition.

In general, co-solvents with weaker binding energy to  $\text{Li}^+$  and lower dielectric constants significantly regulate the interaction between anion and cation by providing a specific low-dielectric condition. Thus, Huang et al. clarified that the non-solvent and low-dielectric co-solvents can essentially regulate the interaction between anion and cation.<sup>[25]</sup> Due to the

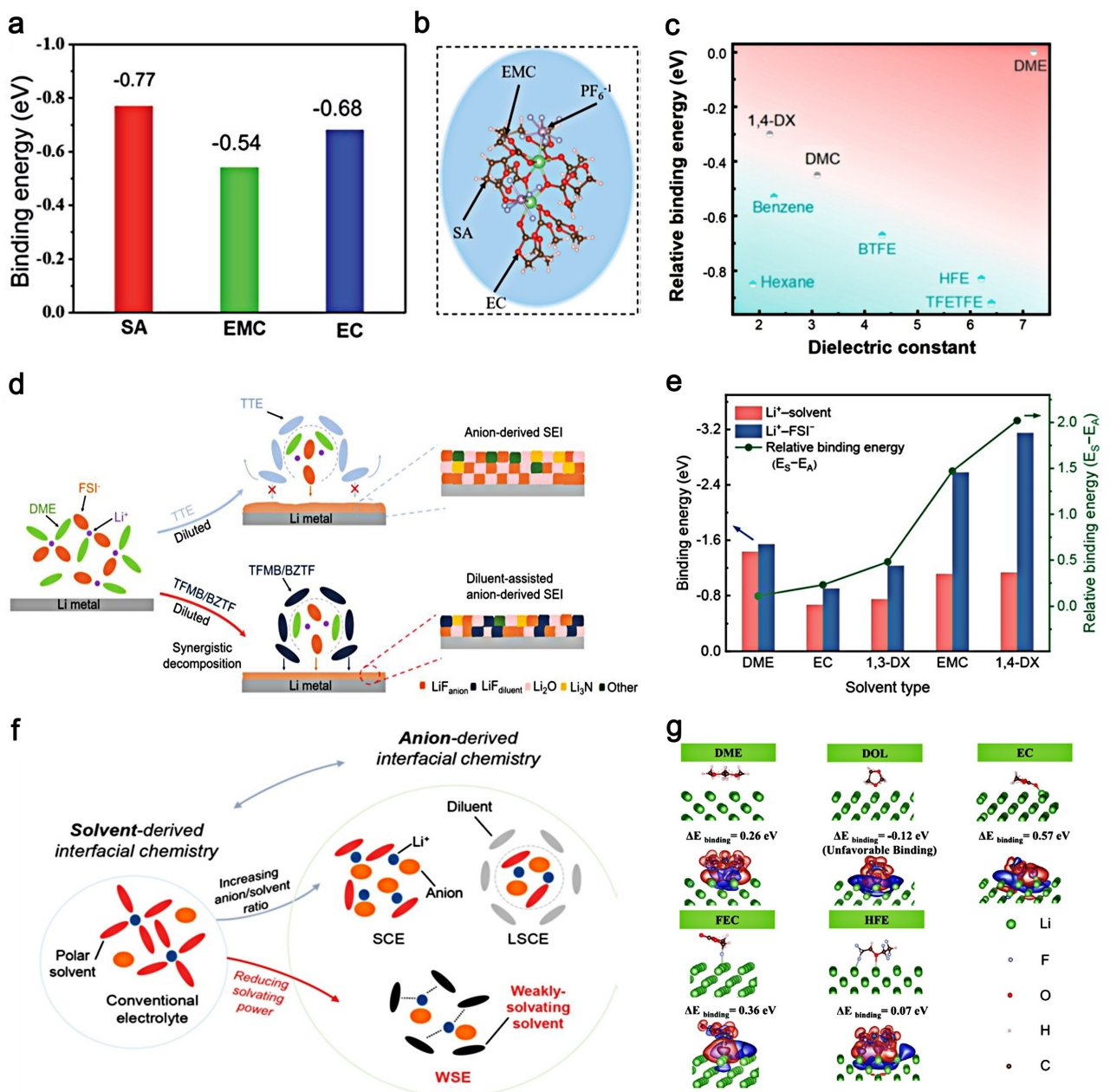


**Figure 2.** a) Calculated binding energies for  $\text{Li}^+/\text{SA}$ ,  $\text{Li}^+/\text{EMC}$ , and  $\text{Li}^+/\text{EC}$ . b) Representative Li-solvation structure in the SA-containing electrolyte. Reproduced with permission from Ref. [24]. Copyright (2021) The Royal Society of Chemistry. c) The solvent diagram with regard to relative binding energy towards  $\text{Li}^+$  and dielectric constant. Reproduced with permission from Ref. [25]. Copyright (2021) Wiley-VCH. d) Schematic diagram of the electrolyte structure and the correspondingly formed SEI in TTE-diluted and TFMB/BZTF-diluted HCEs. Reproduced with permission from Ref. [26]. Copyright (2022) American Chemical Society. e) The binding energies between  $\text{Li}^+$  and solvents/anions obtained by first-principles calculations. f) The solvation structures in the conventional electrolyte, super concentrated electrolyte (SCE), localized super concentrated electrolyte (LSCE), and weakly solvating electrolyte (WSE). Reproduced with permission from Ref. [27]. Copyright (2020) Wiley-VCH. g) Theoretical calculation of the binding energy and charge density of different solvents on Li metal. Reproduced with permission from Ref. [28]. Copyright (2021) Elsevier B.V.

introduction of the low-dielectric co-solvent, the resulting massive positively charged anionic-cation aggregates are prior to the Li metal anode, inducing binding energy derived inorganic-rich SEI layer. A solvent map was also established to clarify that the solvents with suitable binding energies and dielectric constants are matching as low-dielectric co-solvents in Figure 2(c).

Fan et al. presented a kind of LHCEs by adding fluorinated aromatic diluents into HCEs.<sup>[26]</sup> Figure 2(d) shows a principle scheme of the formation of SEI layer in lithium bis(fluorosulfonyl)imide (LiFSI)-trifluoromethoxybenzene (TFMB)/benzotrifluoride (BZTF) during Li plating. Unlike 1,1,2,2-tetrafluoroethyl-2,2,3,3-tetrafluoropropyl ether (TTE), which does not decompose on the anode, the TFMB/BZTF diluent is partially decomposed together with the FSI<sup>-</sup>, participating in

the formation of SEI layer. This synergy through the pairing anionic diluents is expected to have important implications for optimizing electrochemical property.

Zhang et al. systematically researched a weakly solvating electrolyte (WSE) electrolyte and the derived interphase chemistry on electrodes in Figure 2(e and f).<sup>[27]</sup> Significantly, the 1,4-dioxane solvent achieves ultra-low solvating power and regulates Li salts solubility. The spectroscopy results show that the WSE electrolyte exhibits a distinct solvated structure with ion pairs and aggregates at the standard 1 M Li salt concentration. First-principles calculations reveal that the relative binding energies between solvents and  $\text{Li}^+$  determine the electrode/electrolyte interphase chemistry, opening a new avenue for electrolyte design in future LIBs.

Xia et al. revisited the design criteria of advanced SEI on the Li metal anode.<sup>[28]</sup> The density functional theory (DFT) calculation results show that compared with the ether molecule, the carbonate molecule is more likely to react with Li metal, resulting in excess organic components in the SEI layer. On this basis, an advanced SEI design method is proposed by optimizing the composition of carbonate rock electrolytes. The designed SEI layer has a multi-layer structure, where the inorganic layer is dense, and the organic outer layer is ultra-thin.

## 2.2. CEI derived from binding energy

As shown in Figure 3(a and b), Xu et al. reported the research on the influence of ether-based HCEs and LHCEs systems corresponding to the CEI composition of  $\text{LiNi}_{0.8}\text{Co}_{0.1}\text{Mn}_{0.1}\text{O}_2$  (NCM811) cathode.<sup>[30]</sup> In HCE system, the LiF-rich CEI is dependent on the  $\text{FSI}^-$  anion, leading to the decomposition of cathode transition metal ions. In contrast, the fluorinated ether in LHCEs is not an "inert" diluent, which greatly affects the formation of CEI layer.

Borodin et al. investigated the electrochemical capability and mechanistic effects of two various salts of lithium bis(fluorosulfonyl)imide ( $\text{Li}_2\text{FSI}$ ) and lithium bis-trifluoromethane sulfonimide ( $\text{Li}_2\text{TFSI}$ ) doped in ether electrolytes from molecular-scale simulations and experiments.<sup>[31]</sup> The DFT calculations reveal complex interactions between  $\text{FSI}^-$  and  $\text{TFSI}^-$  on the electrode/electrolyte interphase layer and stabilizing CEI interface in Figure 3(c).

In addition, Qiu et al. clarified that the decomposition of the iron ion is the main reason for the low CE of lithium-rich materials.<sup>[32]</sup> Furthermore, they proposed a method to suppress the dissolution of the iron ion by the homogeneous and robust LiF-rich CEI layer, in stark contrast to the heterogeneous and crumbly organic-rich CEI layer in the dilute electrolyte in Figure 3(d and e).

Yang et al. used the synergistic effect of modified electrolytes with nitrile suberonitrile (SUN), 1,3,6-hexanetrinitrile (HTCN) and fluoroethylene carbonate (FEC) as auxiliary agents to design ultrathin and uniform interfacial layers on  $\text{LiCoO}_2$  cathodes.<sup>[33]</sup> They further applied DFT calculations at the atomic scale. The binding energies of succinonitrile (SN), adiponitrile

(ADN), SUN, and HTCN on  $\text{LiCoO}_2$  (1 0 –1 4) surfaces are compared in Figure 3(f), respectively. The results show that SUN and HTCN tend to adsorb horizontally on the  $\text{LiCoO}_2$  surface, which is more favorable for the formation of thinner and more stable CEI films than the vertical adsorption of SN and ADN. It can be seen from Figure 3(f) that the binding energies of SUN (–0.63 eV) and HTCN (0.65 eV) on the surface of  $\text{LiCoO}_2$  (1 0 –1 4) are both lower than those of EC (0.29 eV) and FEC (0.34 eV), indicating that the first two solvents are beneficial to  $\text{LiCoO}_2$  surface adsorption. The strong binding energy of the SUN and HTCN can effectively inhibit the bonding of cobalt and carbonyl oxygen on the surface of EC and FEC, thereby stabilizing the microstructure of the electrode surface. Through spectroscopic analysis and theoretical calculation, the adsorption coordination mechanism of the nitro group and cobalt and the synergistic effect of auxiliary agents were discussed.

The rapid growth of Li dendrites and the decomposition of electrolytes at the interface during charging limit the cycle life and hinder the application of Li metal batteries. Here, Ma et al. developed a nonflammable triethyl phosphate (TEP) electrolyte with tris(hexafluoroisopropyl)phosphate (THFP) as additive.<sup>[34]</sup> The polar nature of the C–F bond and the abundant  $\text{CF}_3$  groups in THFP reduce its LUMO energy and the highest occupied molecular orbital (HOMO) energy, which helps form a stable, LiF-rich SEI by reducing THFP, which increases the incorporation of  $\text{PF}_6^-$  anions. Furthermore, the polarized  $\text{CF}_3$  groups in THFP have the highest binding energy for  $\text{PF}_6^-$  adsorption (Figure 3g), which increases the dissociation of  $\text{LiPF}_6$  and the mobility of  $\text{Li}^+$  by reducing the interaction of  $\text{Li}^+$  with  $\text{PF}_6^-$ . The strong interaction of THFP- $\text{PF}_6^-$  suppresses the released  $\text{PF}_6^-$  movement, releasing more  $\text{Li}^+$  for ion transport. In addition, THFP also participates formation of a thin, C–F rich CEI layer to provide stable cycling of the cathode under high voltage. Symmetrical  $\text{Li}||\text{Li}$  and intact  $\text{Li}||\text{NCM}622$  cells with THFP addition are characterized by small polarization and long cycle life, which illustrates the importance of THFP additives for the application of LIBs.

In summary, the electrode/electrolyte interphases play a critical role in enhancing the cyclability and prolonging the service life of rechargeable LIBs to meet the sustainable energy requirement of the mobile society. Thus, tailoring binding energy between  $\text{Li}^+$  and solvents can dominate the formation process, structure, and chemical composition of the interface. In addition, the analysis of binding energy of low solvation electrolytes sheds light on the fundamental understanding of SEI and CEI layers. It provides a scientific and rational principle for the design of the electrode/electrolyte interphases and long-term cycle rechargeable LIBs.

## 3. Activation Energy and Process of Solvation/De-solvation

Traditional liquid electrolytes applied in rechargeable batteries and electrochemical capacitors consist of solvents, anions, and

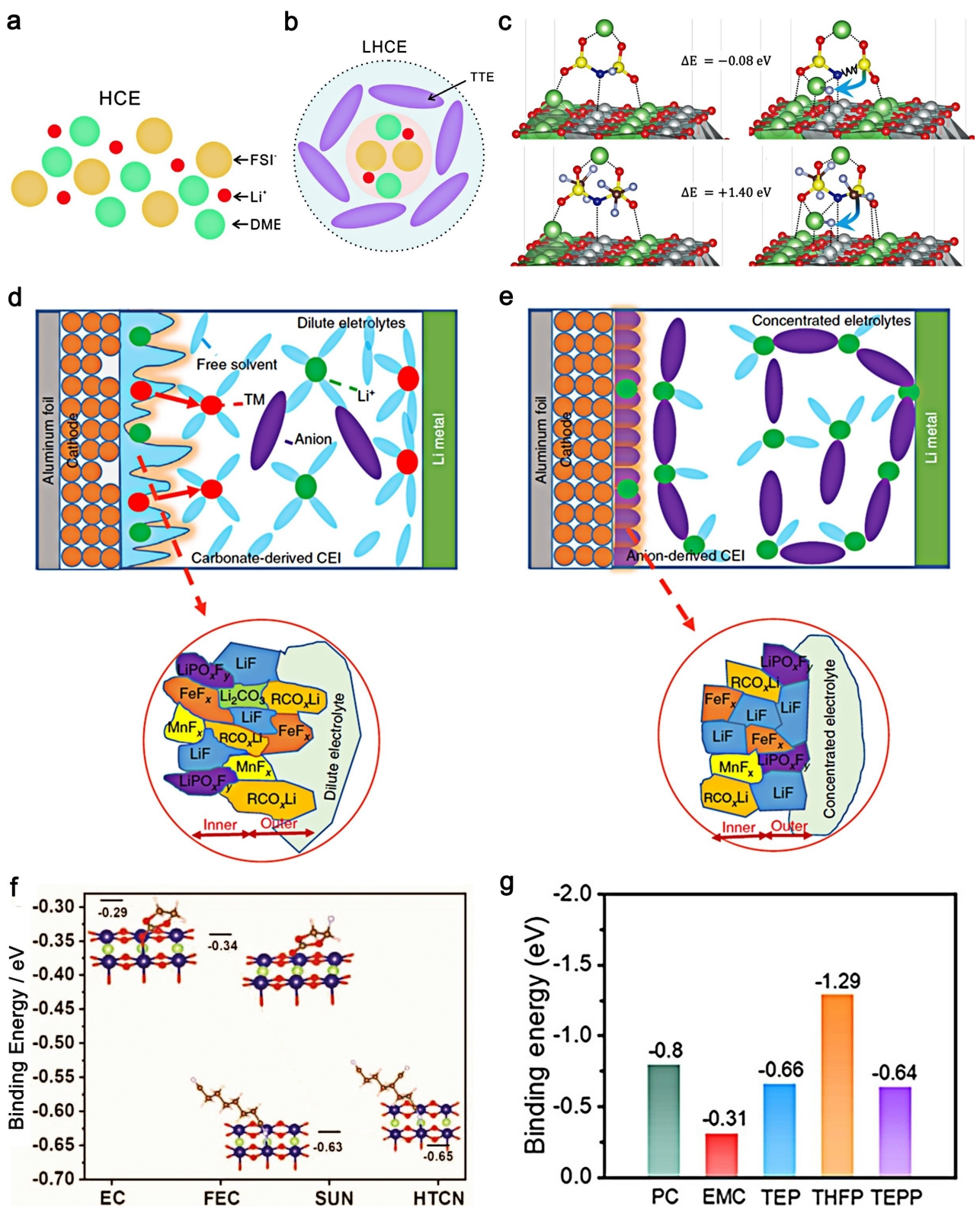


**Figure 3.** a) The scheme of the solvation structure in the HCE (LiFSI-1.2 DME). b) The scheme of the solvation structure in the LHCE (LiFSI-1.2 DME-3 TTE). Reproduced with permission from Ref. [30]. Copyright (2019) Elsevier B.V. c) Reaction mechanism of  $\text{Li}^+\text{FSI}^-$  and  $\text{Li}^+\text{TFSI}^-$  on  $\text{LiNiO}_2$  (1 0 4) surface. Reproduced with permission from Ref. [31]. Copyright (2019) The Royal Society of Chemistry. d and e) Schematic illustrations of passivation films in 1 and 3 M electrolytes. Reproduced with permission from Ref. [32]. Copyright (2020) Springer Nature. f) Comparison of binding energies of EC, FEC, SUN, and HTCN on the (1 0 1 4) surface of  $\text{LiCoO}_2$ . Reproduced with permission from Ref. [33]. Copyright (2020) Wiley-VCH. g) The binding energy between the solvents/additives and  $\text{PF}_6^-$ . Reproduced with permission from Ref. [34]. Copyright (2022) Elsevier B.V.

solvent-solvated cations, following the classic “solvated cation” electrolyte configuration.<sup>[35]</sup> In most electrolytes, the de-solvation process of solvated cations occurs when the cations are de-solvated, intercalated, and deposited on the electrode surface.<sup>[36]</sup>

### 3.1. Activation energy regulating solvation degree

Understanding the activation energy barrier during the Li<sup>+</sup> intercalation process in cathode and anode materials is significant for advancing high-performance LIBs. Kislenko et al. proposed an alternative model of the activation barrier for

intercalation that derives from the nature of solvents and electrode materials in Figure 4(a–c).<sup>[37]</sup> Combining with experimental verification and classical molecular dynamics simulations, they achieved that the rate-limiting step of Li<sup>+</sup> de-solvation process is affiliated with the Li<sup>+</sup> crossing the electrode/electrolyte interphase.

Furthermore, Li et al. calculated the activation energy ground on the electrochemical impedance spectroscopy.<sup>[38]</sup> As shown in Figure 4(d–f), once the electrochemical reaction takes place, EC, diethyl carbonate (DEC) molecules, and hexafluorophosphate ion (PF<sub>6</sub><sup>-</sup>) are reduced by the electron in the Li<sup>+</sup> solvated sheath to form the organic-based SEI. The outer SEI layer comprises EC or DEC solvent-derived organic components

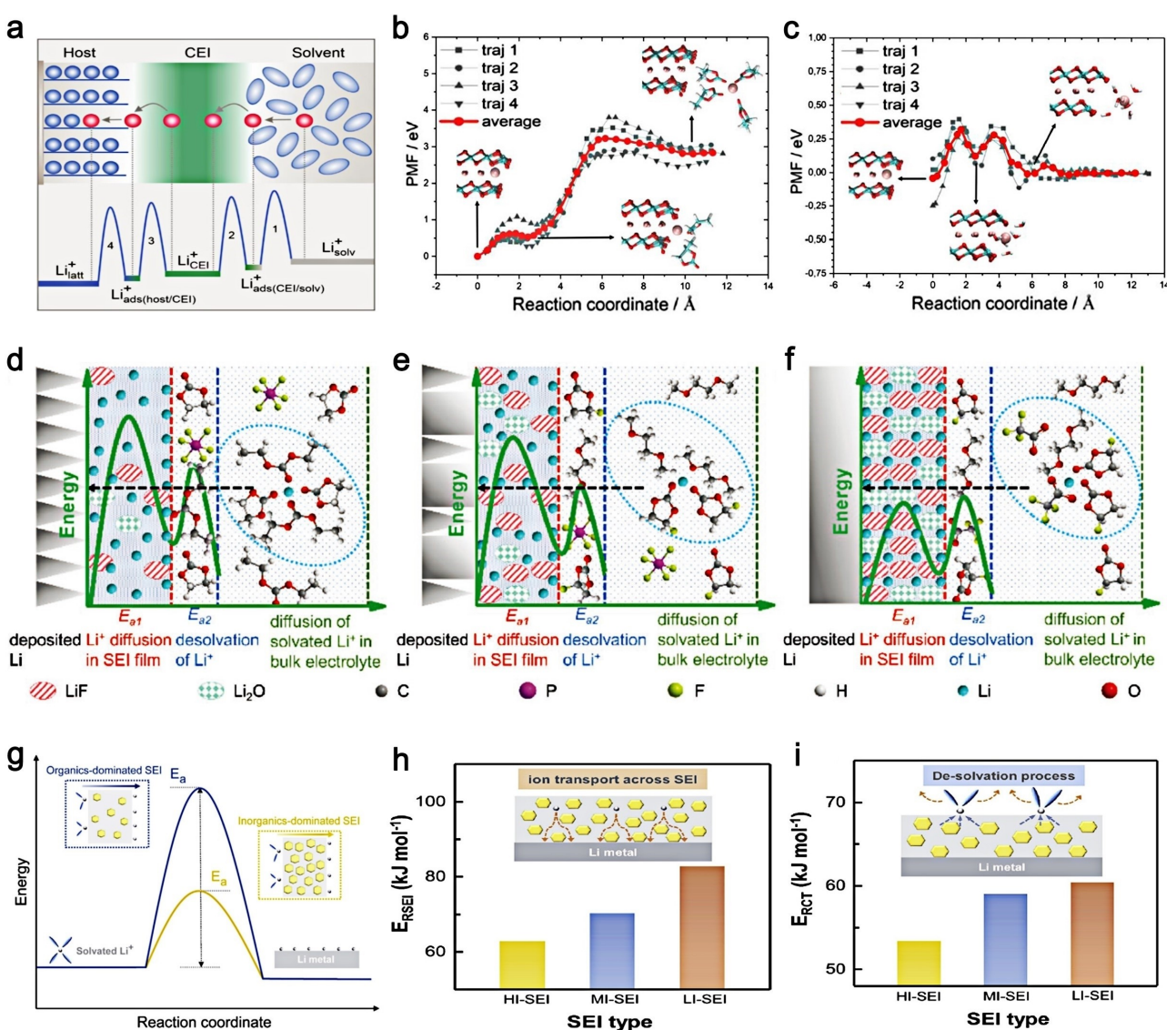


**Figure 4.** a) Schematics of the Li-ion intercalation into a layered host. Potential of mean force profiles for the b) LiCoO<sub>2</sub>/PC and c) LiCoO<sub>2</sub>/H<sub>2</sub>O systems and the snapshots of ions in the solvated states, adsorbed states, and the host lattice in the vicinity of the LiCoO<sub>2</sub> surface. Reproduced with permission from Ref. [37]. Copyright (2021) Elsevier B.V. Schematics of the Li<sup>+</sup> deposition process in different electrolytes d) LiPF<sub>6</sub>-EC/DEC, e) LiPF<sub>6</sub>-DME/FEC, and f) LiTFA-DME/FEC. Reproduced with permission from Ref. [38]. Copyright (2020) Wiley-VCH. g) A schematic illustration that an inorganics-rich SEI contributes to a lower  $E_a$  for the interfacial journey of Li<sup>+</sup>, which is linked with Li-ion de-solvation and subsequent ion diffusion across SEI. Comparisons of activation energy for decoupled processes of h) ion transport across SEI ( $E_{RSEI}$ ) and i) de-solvation ( $E_{RCT}$ ) with regard to HI-SEI, MI-SEI, and LI-SEI by fitting the  $R_{SEI}$  and  $R_{CT}$  obtained under various temperatures (−20~30 °C) with Arrhenius equation. The insets are the respective schematic illustrations of ion diffusion across SEI and de-solvation process. Reproduced with permission from Ref. [39]. Copyright (2020) Elsevier B.V.

$\text{ROCO}_2\text{Li}$ , while the inner layer is mainly composed of  $\text{Li}_2\text{O}$  and  $\text{LiF}$ . Firstly,  $\text{Li}^+$  needs to cross a large energy barrier ( $97.91 \text{ kJ mol}^{-1}$ ) to leave the  $\text{Li}^+$  solvent sheath before the deposition process. Secondly, the highly resistive organic  $\text{ROCO}_2\text{Li}$  species with a large energy barrier ( $69.14 \text{ kJ mol}^{-1}$ ) hinders the  $\text{Li}^+$  diffusion and induces an inhomogeneous charge distribution as  $\text{Li}^+$  transports through the SEI, giving rise to the Li dendritic growth. Since the solvation of FEC is weaker than that of EC, the energy barrier ( $64.92 \text{ kJ mol}^{-1}$ ) for  $\text{Li}^+$  de-solvation is slightly reduced with dimethoxyethane (DME)/FEC solvents. The  $\text{Li}^+$  diffusion barrier ( $89.76 \text{ kJ mol}^{-1}$ ) across the SEI is also reduced, probably due to the increased  $\text{LiF}$  content from the addition of FEC and  $\text{PF}_6^-$ , which enhances the  $\text{Li}^+$  transport kinetics and produces inconspicuous dendritic morphologies. In contrast, trifluoroacetate ion ( $\text{TFA}^-$ ) regulates the solvation environment of the  $\text{Li}^+$ , promoting fast de-solvation process ( $60.02 \text{ kJ mol}^{-1}$ ). Furthermore,  $\text{LiF}$  and  $\text{Li}_2\text{O}$  are beneficial for the uniform diffusion field gradient and stabilizing the SEI film, contributing to a small energy barrier ( $59.66 \text{ kJ mol}^{-1}$ ) for  $\text{Li}^+$  to transport through SEI.

Huang et al. systematically investigated the interfacial transfer kinetics model of solvated  $\text{Li}^+$  for various SEIs in Figure 4(g).<sup>[39]</sup> The correlation between the inorganic-abundant SEI and solvated interface forms a lower energy barrier, which involves a simple de-solvation process and fast ion diffusion through the SEI. Due to the low interfacial energy barrier ( $53.4 \text{ kJ mol}^{-1}$ ) of the inorganic-abundant SEI, the overpotentials for both the initial nucleation of Li and the interfacial activation process are the lowest among the various SEIs, contributing to the formation of dense Li properties.

### 3.2. Process and location of solvation/de-solvation

The charge transfer process is the primary reaction of rechargeable LIBs. Predicting the energy change of charge transfer reactions from DFT calculations is necessary to enable the design of electrolyte/electrode interfaces. However, the microstructure and composition are often hard to explore in operation conditions. Therefore, Qi et al. described the energy diagram of the equilibrium and kinetics of the electrochemical reaction in Figure 5(a).<sup>[40]</sup> Using DFT and density functional-based tight binding (DFTB) calculations, a novel model was exploited for predicting the energy distribution of lithiation and de-lithiation charge transfer reactions at the interphase. The results show that  $\text{Li}^+$  is more preferentially dissolved on a zero-charge Li anode, indicating that the SEI layer is an inevitable barrier to prevent  $\text{Li}^+$  from completely dissolving into the electrolyte.

Two processes are required before  $\text{Li}^+$  gains electrons and deposits into the current collector (Figure 5b): the de-solvation process of  $\text{Li}^+$  and the  $\text{Li}^+$  crossing the SEI layer. By comparison, Xu et al. successfully differentiated the contributions of the intercalation process of  $\text{Li}^+$  in graphite and lithium titanium oxide (LTO) anodes, with the de-solvation of solvated  $\text{Li}^+$  and naked  $\text{Li}^+$  through SEI.<sup>[41]</sup> The energy barrier calculation results show that the de-solvation of solvated  $\text{Li}^+$  is the rate-

determining step, where the activation energy is  $50 \text{ kJ mol}^{-1}$ . In contrast, the migration energy barrier of bare  $\text{Li}^+$  through SEI is merely  $20 \text{ kJ mol}^{-1}$ . This result suggests that it is essential to manipulate the interfacial science to sufficiently dissociate solvent molecules from the original solvation structure of  $\text{Li}^+$ .

Zhou et al. found a novel kind of electrolyte<sup>[36]</sup> by transferring the ordinary de-solvation process from the surface of the electrode to the metal-organic framework (MOF) channels in Figure 5(c). By transferring the de-solvation process of solvated  $\text{Li}^+$  from the surface of the reaction electrode and regulating the free solvent molecules and de-solvation to an inactive "frozen-like" state, they effectively reduce their reactivity and prevent solvent decomposition issues. Unlike traditional liquid electrolytes, this new electrolyte consists only of inactive frozen solvent, and the de-solvated  $\text{Li}^+$  constitutes crystalline lithium salt solute. The results show that the electrochemical stability of this " $\text{Li}^+$  de-solvated ether-based electrolyte" is significantly improved (expanded from  $3.8 \text{ V}$  to  $4.5 \text{ V}$ ). An ultra-stable high-energy-density lithium metal battery (NCM811//Li) is obtained. It is also surprising that there is no CEI layer on the surface of cycled NCM811, owing to the  $\text{Li}^+$  de-solvated electrolyte.

Ming et al. presented a novel solvation structure and interfacial model between the  $\text{Li}^+$  and solvents at the electrode/electrolyte interphases to determine the process of solvation/de-solvation (Figure 5d).<sup>[42]</sup> A novel carbonate-based high-voltage electrolyte is reported using a mixed solvent of ethyl methyl carbonate (EMC) and methyl acetate (MA) without any additives. At the normal concentration of  $1.2 \text{ M LiPF}_6$ , the electrolyte successfully achieves excellent stability, fast charging capability, and superior low-temperature performance. The results show that the interaction of  $\text{Li}^+$ , anions, and solvent is crucial in determining the interfacial behavior between the electrolyte and the electrode. More importantly, they propose a groundbreaking interfacial model related to the solvated structure of  $\text{Li}^+$ , revealing the molecular-scale interactions of  $\text{Li}^+$ -solvent-anions on the electrode surface and their impact on battery performances.

### 3.3. Solvation/de-solvation process for low-temperature battery

Given that the conventional graphite anode suffers from the slow diffusion kinetics, high reaction energy barrier of  $\text{Li}^+$  in the interlayers, large interfacial resistance, and the unstable SEI forming in the catastrophic lithium plating process at ultra-low temperature,<sup>[43]</sup> the lowest operating temperature of commercial graphite anode is limited to  $\sim -20^\circ$ .<sup>[44]</sup> In contrast, Li metal with the lowest electrochemical potential, ideally host-less nature, and low reaction energy barrier as the anode can effectively reduce the polarization effect and realize the normal operation through a conversion reaction, which has been expected to meet the low-temperature operation.<sup>[30,45]</sup> Therefore, the low-temperature utilization of new lithium batteries has received extensive attention in recent years.<sup>[46]</sup> The weak solvation structure of  $\text{Li}^+$  will reduce the coordination number

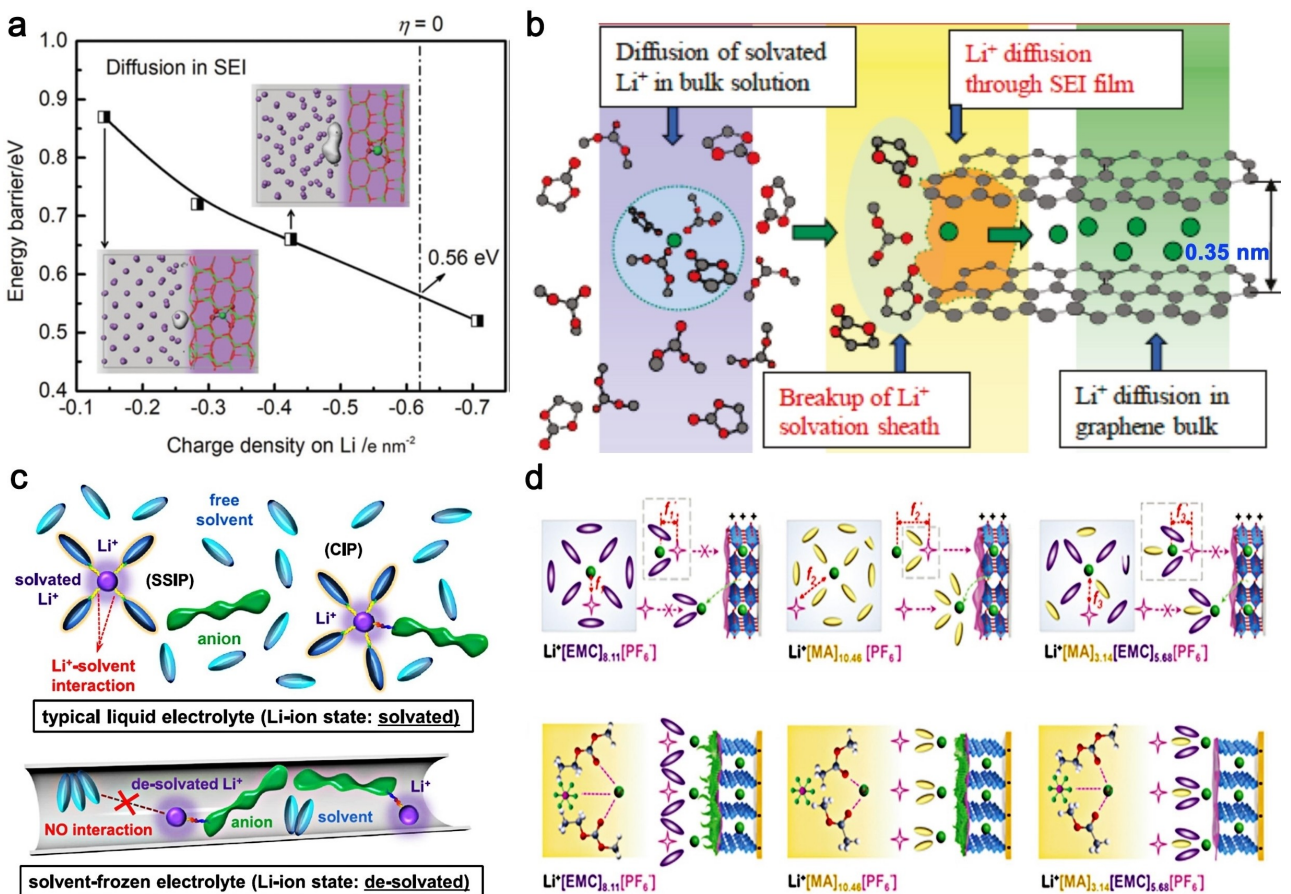


**Figure 5.** a) The energy barriers of a Li<sup>+</sup> to form and transport in the Li<sub>2</sub>CO<sub>3</sub> at the Li/Li<sub>2</sub>CO<sub>3</sub>/EC interface as a function of charge density on the Li-metal electrode. Reproduced with permission from Ref. [40]. Copyright (2019) The Royal Society of Chemistry. b) Schematic description of energetic coordinates for Li<sup>+</sup> transfer at graphite/electrolyte junction. Reproduced with permission from Ref. [41]. Copyright (2010) American Chemical Society. c) A new electrolyte design concept that will redefine the configuration of liquid electrolytes: liquid electrolyte with de-solvated lithium ions. Reproduced with permission from Ref. [36]. Copyright (2020) Elsevier B.V. d) Interfacial behavior and simulation from the bulk electrolyte to electrode interphase. Reproduced with permission from Ref. [42]. Copyright (2021) Wiley-VCH.

of Li<sup>+</sup> and de-solvation energy, thereby improving the transportability of Li<sup>+</sup> in low-temperature environments and enhancing the discharge capacity of low-temperature LIBs. Nevertheless, the development of low-temperature LIBs has always been caught in a dilemma of electrolyte system selection, which plays an irreplaceable role in realizing the chemical reaction in LIBs.<sup>[45a,47]</sup> Therefore, widespread efforts have been dedicated to modifying the architecture of electrolytes to match with advantageous and high energy density batteries at low temperatures.

LIBs operating at  $-70^{\circ}$  are achieved using ethyl acetate (EA)-based solvents, but the battery voltage is limited to  $\sim 2$  V.<sup>[48]</sup> After introducing “inert” dichloromethane (DCM), the solvation structures did not change (Figure 6a), neither dissolving salts nor destroying the original solvation structures, resulting in LHCEs with co-solvated structures. In the earliest days, Meng et al. combined high dielectric-fluidity factor and used liquefied gas electrolyte, enabling Li||LiCoO<sub>2</sub> LIBs (3.5 V  $\sim$  4.1 V) to keep about 60% of the room temperature capacity within ten cycles at  $-60^{\circ}$ .<sup>[53]</sup> Compared with commercial solvents, the liquefied gas solvents own a higher dielectric-

fluidity factor, which corresponds with a lower dielectric constant (10~15) and small viscosity. The superior physical properties reduce the coordination of Li<sup>+</sup> with liquefied gas solvents, improving the transportability of Li<sup>+</sup> in low-temperature electrolytes. To further expand the operating temperature range, they presented acetonitrile (AN) as a co-solvent and modified liquefied gas electrolyte (1.2 M LiTFSI + 1 M AN in fluoromethane (FM):CO<sub>2</sub>=19:1) in Figure 6(c), which exhibits excellent stability for Li anodes, enabling Li||NCM622 cells to operate from  $-60^{\circ}$  to  $55^{\circ}$ .<sup>[49]</sup> However, a strategy like this sacrifices the energy density, power density, and safety of batteries at the same time because the battery will have to withstand the high pressures of dozens of bars (Figure 6b), electrolyte low-oxidation defect, and SEI instability.

Non-polar electrolytes are also used for electrode stabilization by decreasing the number of free solvents and manipulating the composition of the interfacial phase. However, non-polar electrolytes will inevitably bring about the issues of low Li<sup>+</sup> conductivity and slow down the transport of Li<sup>+</sup>. For instance, the fluorine-containing non-polar diluent (1,1,2,2-tetrafluoroethyl-2',2',2'-trifluoroethyl ether, HFE) in the opti-

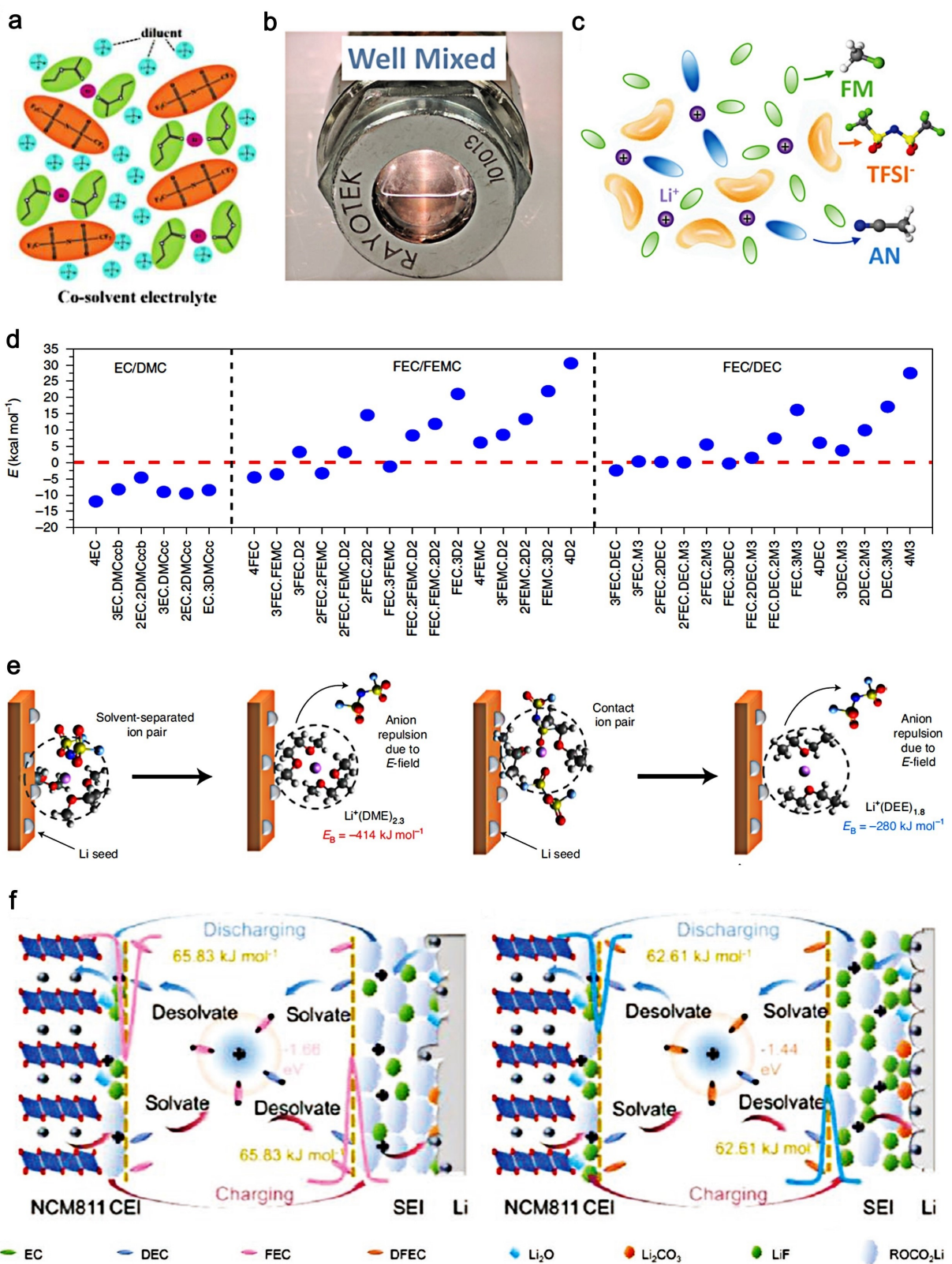


**Figure 6.** a) Schematic images to illustrate the solvation structure of co-solvent electrolyte. Reproduced with permission from Ref. [48]. Copyright (2019) Wiley-VCH. b) Design and conductivity of liquefied gas electrolyte solubility test in a window cell of 1.2 M LiTFSI, 1 M AN in FM. c) Schematic illustration of the solvation structure of the liquefied gas electrolyte. Reproduced with permission from Ref. [49]. Copyright (2020) The Royal Society of Chemistry. d) The calculated  $\text{Li}^+$  solvation/de-solvation energy with different structures of the  $\text{LiPF}_6$ -EC/DMC and super electrolytes. Reproduced with permission from Ref. [50]. Copyright (2019) Springer Nature. e) Proposed de-solvation mechanisms and corresponding  $\text{Li}^+$ /solvent binding energies obtained from quantum chemistry simulations in 1 M LiFSI DOL/DME and 1 M LiFSI DEE. Reproduced with permission from Ref. [51]. Copyright (2021) Springer Nature. f) Schematics of the dynamic evolution of  $\text{Li}^+$  solvation sheath during charging/discharging processes in various electrolytes. Reproduced with permission from Ref. [52]. Copyright (2021) Wiley-VCH.

mized ratio of fluorinated electrolyte is compatible with LIBs and exhibits excellent performance at a low temperature of  $-85^{\circ}$ .<sup>[50]</sup> Non-polar solvents break the strong interactions between highly polar molecules, enlarge the liquid phase range and increase the transfer number. The  $\text{Li}^{+}$  solvation/de-solvation energies for conventional carbonate electrolytes and disassociated electrolytes were calculated and compared in Figure 6(d). The lower ion de-solvation energy in the electrolyte is crucial for the kinetic performances because the solvent molecules around the  $\text{Li}^{+}$  must be completely stripped before intercalating into the electrode. Especially at low temperatures, the slow de-solvation process of  $\text{Li}^{+}$  greatly limits the lithiation/de-lithiation reaction kinetics. By introducing FEC/FEMC or FEC/DEC polar solvent into the non-polar solvent (tetrafluoro-1-(2,2,2-trifluoroethoxy)ethane (D2) or methoxyperfluorobutane (M3), the complexes involving D2 and M3 molecules can further enhance the solvation energy due to the weak interaction between  $\text{Li}^{+}$  and D2 or M3 solvent molecules.

Ether-based electrolytes with low  $\text{Li}^{+}$  de-solvation energy exhibit excellent stability toward Li metal anode due to the low reduction potential and formation of anion-derived SEI. Liu et al. built a solvated structure of  $\text{Li}^{+}$  for the reversibility and electro-plating behavior of Li metal at low temperatures in Figure 6(e).<sup>[51]</sup> The de-solvation behavior directly describes the performance difference between 1,3-dioxolane (DOL)/DME-based and diethyl ether (DEE) systems. Analysis of radial distribution function (RDF) data shows that DOL/DME and DEE electrolytes display distinctive solvent-separated pair (SSIP) and contact-ion pair (CIP) structures, in which the  $\text{Li}^{+}$  coordination number of DME and DEE are 4.6 and 1.8.

In addition, the ionic dipole can directly affect the  $\text{Li}^{+}$  de-solvation process and the formation of passivation layers, leading to a uniform Li deposition morphology. The slow evolution of the  $\text{Li}^{+}$  solvation structure results in a high charge transfer barrier and a high  $\text{Li}^{+}$  diffusion barrier, which leads to unsatisfactory Li dendrites and capacity loss in LIBs. Therefore, an ionic dipole strategy was introduced to accelerate the evolution of the  $\text{Li}^{+}$  solvation structure by adjusting the degree of fluorination of the solvating agent. From FEC to difluoroethylene carbonate (DFEC), the coordination ratios (0.76 to 0.69) and ionic-dipole interaction strengths (1.66 to 1.44 eV) decrease with an increasing tendency of fluorination, as shown in Figure 6(f).<sup>[52]</sup> Therefore, at  $-20^{\circ}\text{C}$ , the  $\text{Li}^{+}$  de-solvation rate of the DFEC-based electrolyte is six times that of the fluorine-free EC-based electrolyte.

In summary, the solvation and de-solvation energy is the best reflection of the rate-determining step of electrolytes. The transference of  $\text{Li}^{+}$  is mainly divided into the following parts, including the formation of  $\text{Li}^{+}$  solvation sheath,  $\text{Li}^{+}$  being absorbed on SEI/CEI layers,  $\text{Li}^{+}$  de-solvation process,  $\text{Li}^{+}$  crossing SEI/CEI layers, and  $\text{Li}^{+}$  combining with anode and cathode. By regulating the solvation and de-solvation energy of  $\text{Li}^{+}$ , the energy barrier of  $\text{Li}^{+}$  diffusion can be reduced, resulting in low nucleation over potential, fast ion transference kinetics, uniform deposition of  $\text{Li}^{+}$ , and favorable electrochemical performance. This section sheds light on the relations between SEI/CEI layer properties and the solvation and de-solvation

energy of  $\text{Li}^{+}$  and provides more fundamental insights into the solvation and de-solvation process for stable low-temperature working batteries.

## 4. Structure of Solvent

The various distribution and transport characteristics of  $\text{Li}^{+}$  in the electrode/electrolyte interphase region of Li metal anode directly determine the deposition behavior of  $\text{Li}^{+}$ .<sup>[7a]</sup> Novel electrolyte formulation alters the  $\text{Li}^{+}$  solvation environment for uniform Li deposition morphology, SEI stability, and high CE.<sup>[54]</sup> A general conclusion about the solvation coordination structure is that the binding energy between the oxygen atom and the cation and the spatial structure of the solvent molecule plays a crucial role in improving the cycling performance of LIBs.

### 4.1. Diverse structure of novel solvents

Bao et al. synthesized a group of fluorinated-1,2-diethoxyethanes aiming at high-rate capability and high ionic conductivity of electrolytes in Figure 7(a).<sup>[55]</sup> It was found that the position and number of F atoms on 1,2-diethoxyethane exhibit a remarkable influence on the electrolyte property. Partially fluorinated locally polar  $\text{CHF}_2$  is identified as the optimal group, rather than fully fluorinated  $\text{CF}_3$  in common designs. In addition, the  $\text{Li}^{+}$  and solvent binding energies, the geometry of electrolytes, and the solvation coordination environment are closely related to the ionic conductivity and overpotential of the battery. Therefore, they further designed and synthesized 1,6-dimethoxyhexane (FDMH),<sup>[56]</sup> which has a longer  $-\text{CF}_2-$  backbone than 1,4-dimethoxybutane (FDMB) in Figure 7(b).<sup>[57]</sup>

Wang et al. proposed a partially fluorinated ether of bis(2,2-difluoroethyl) ether (BDE) as a functional co-solvent to form a novel LHCEs system for dendrite-free and long-cycle LIBs.<sup>[58]</sup> The BDE co-solvent acts as a diluent to dissociate Li salts through weak interactions, reducing electrolyte viscosity and increasing  $\text{Li}^{+}$  conductivity to 6.4 mS/cm in Figure 7(c). Besides, the BDE co-solvent promotes the formation of a uniform LiF-rich SEI and suppresses the deposition of Li dendrites by modulating the solvent shell structure, leading to a high CE of 99.6%.

Lu et al. introduced Tin (II) trifluoromethanesulfonate as a solubilizer into 1 M  $\text{LiPF}_6$  in EC/DEC commercial carbonated electrolyte to resist the solvation barrier of  $\text{LiNO}_3$ .<sup>[59]</sup> The metal-organic hybrid SEI layer derived from the  $\text{Sn}^{2+}-\text{NO}_3^-$  coordination solvation structure has an aspiring effect on the grain coarsening of Li deposition in Figure 7(d). Cheng et al. introduced the  $\text{LiNO}_3$  and a small number of tetramethylurea (TMU) as a multi-functional co-solvent into the commercial carbonate electrolyte,<sup>[60]</sup> which can facilitate normally insoluble  $\text{NO}_3^-$  into the solvated structure of  $\text{Li}^{+}$  to form a conductive and stable SEI in Figure 7(e). Meanwhile, the

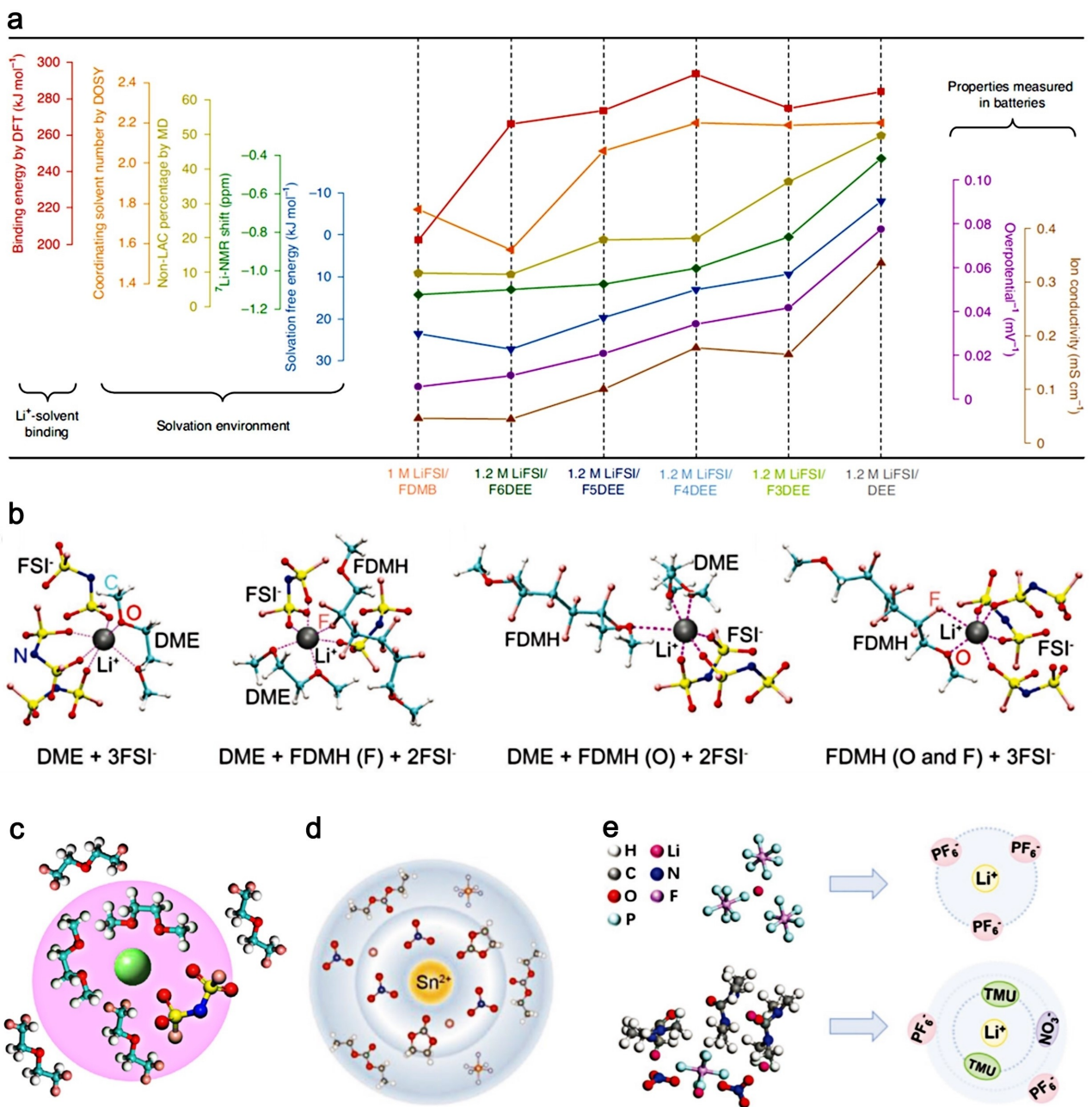


**Figure 7.** a) Structure-property relationship plots of Li<sup>+</sup>-solvent binding, solvation environments, and properties measured in batteries. Reproduced with permission from Ref. [55]. Copyright (2022) Springer Nature. b) Different types of Li-ion solvation environments in the 1 M LiFSI/6 FDMH-DME electrolyte through molecule dynamic (MD) simulation. Reproduced with permission from Ref. [56]. Copyright (2021) Wiley-VCH. c) The proposed unique solvation structure of BDE/DME electrolyte. Reproduced with permission from Ref. [58]. Copyright (2022) Elsevier B.V. d) Schematic illustration of the solvation sheath structure in solubilizer-mediated carbonate electrolyte. Reproduced with permission from Ref. [59]. Copyright (2020) Wiley-VCH. e) Representative configurations of the solvation structures of Li<sup>+</sup> in CCE and CCE-TMU/LiNO<sub>3</sub>. Reproduced with permission from Ref. [60]. Copyright (2022) Wiley-VCH.

production of HF is inhibited by regulating the solvation structure and scavenging effect.

In Summary, engineering to improve the degree of solvation in liquid electrolytes is a cost-effective and practical approach to address the root cause, the uncontrollable parasitic reaction between electrodes and electrolytes. To achieve the cyclability, oxidative stability, and ionic conductivity of the electrolyte simultaneously, the solvation capacity of the solvent must be fine-tuned. Achieving a balance between fast ionic

conduction and electrode stability by fine-tuning the solvent's solvation degree is crucial, and meanwhile, molecular design and synthesis tools play an important role. We provide a systematic summary of the structure-property relationships of these electrolytes with multiple theoretical and experimental tools, including cross-validation of key properties such as Li<sup>+</sup>-solvent coordination, solvation structure, and battery performance, and explain in detail their correlations.

## 5. Low-Solvation Electrolytes Derived from Li Salts

An efficient method to design a low-solvation structure is adding Li salts, which is an economical way to improve battery performance. In this section, various Li salts for high energy density cathodes are discussed below. Li salts, such as LiFSI,<sup>[61]</sup> LiTFSI,<sup>[62]</sup> lithium difluoro(oxalato) borate (LiDFOB),<sup>[22c]</sup> and lithium bis(oxalate) borate (LiBOB)<sup>[63]</sup> can also contribute anions to the formation of Li<sup>+</sup> solvated structure, especially in the LHCEs system. The structure of electrolytes varies not only with the kind of solvents and Li salts, but also with the concentration of the Li salts. As the concentration of Li salt increases, more and more solvents participate in the coordination structure, resulting in a rapid reduction of free-flowing solvent molecules. Thereby, the Li<sup>+</sup> has the opportunity to participate in the main solvent shell through ion pairs. Compared with solvent-induced organic-dominated dilute solution SEI/CEI layers, anion-induced inorganic-dominated SEI/CEI layers exhibit significantly faster ion transport and better rate performance. In recent years, the LHCEs system has shown unique advantages in stabilizing Li metal anodes, resulting in stable SEI and CEI with various molar ratios of solvent to Li salt. In the first solvent sheath of LHCEs, the components of SEI and CEI layers that form CIP and aggregated ions are subsequently modulated by anions in LHCEs, termed anion-derived SEI and CEI layers.<sup>[6]</sup> Therefore, the stability and property of anion-derived solvated structure should be preferably improved to break the challenges under different Li salts.

### 5.1. Anion salts compatible with high-voltage cathode

The development of LIBs requires functional electrolytes compatible with high-voltage cathodes and Li metal anodes.<sup>[64]</sup> Li et al. used a moderately concentrated LiPF<sub>6</sub> and LiNO<sub>3</sub> double-salt electrolyte consisting of ester and ether-based FEC/DME co-solvents to form a unique Li<sup>+</sup> weak solvation structure and further stabilize high voltage LIBs.<sup>[65]</sup> Mechanistic studies demonstrate that the weakly solvated structure enhances Li<sup>+</sup> plating/stripping process and induces gradient hetero-structure and high Young's modulus SEI layer, and thin and robust CEI. This electrolyte system with the dual-anion solvation structure regulates a novel insight into interfacial science through solvation modulation.

To conquer the aforementioned problems, Zhang et al. designed a LHCEs system with a non-solvating co-solvent based on LiFSI salt, achieving stable high voltage cathodes, suppressing Al corrosion, and enabling LIBs to operate at a wide temperature.<sup>[71]</sup> Zhang et al. proposed anion receptors to construct the electrolyte structure,<sup>[66]</sup> enabling a stable anion-derived SEI to satisfy high voltage cathodes in Figure 8(a). The tris(pentafluorophenyl)borane (TPFPB) anion acceptor interacts with the electron-deficient boron (B) atom to reduce the reduction stability of FSI<sup>-</sup>. Furthermore, the aggregated cluster

type of FSI<sup>-</sup> in the electrolyte has a change in the presence of TFPPB, and FSI<sup>-</sup> interacts with more Li<sup>+</sup>.

Wang's group reported a high-voltage fluorine-containing electrolyte that supported the most aggressive and high voltage cathodes in LIBs.<sup>[67]</sup> The Li<sup>+</sup> CE of the 5 V LiCoPO<sub>4</sub> cathode (~99.81%) and the NCM811 cathode (~99.93%) indicate the high cycling stability of the battery. The battery capacity keeps around 93% after 1000 cycles with the loading of 2.0 mAh cm<sup>-2</sup>. Surface analysis and quantum chemical calculations demonstrate that the several nanometers' thick fluorinated interfacial phases in Figure 8(b).

Dong et al. reported a rational sulfonamide-based electrolyte capable of stably cycling NCM811 in LIBs with a cut-off voltage as high as 4.7 V.<sup>[68]</sup> As shown in Figure 8(c), the electrolyte suppresses the side reactions, stress corrosion cracking, transition metal dissolution, and resistive growth on the cathode side. The cell provides a capacity of 230 mAh g<sup>-1</sup> and an average CE of 99.65% over 100 cycles.

Lithium-rich layered oxides (LRLO) with a higher theoretical capacity have attracted much attention in recent years for high-energy LIBs. However, the cathode decay and capacity fade hinder the practical application of LRLO during the high-voltage charging process. Thus, the Meng's group added LiBOB salt into the carbonate electrolyte,<sup>[69]</sup> further enhancing the cyclability in high voltage graphite/LRLO full cells. The formation of B-F species was found in the cycling electrolyte, illustrating the scavenging effect of LiBOB on HF in Figure 8(d). Lu et al. added LiDFOB to form a new diluted concentration (LiDFOB/DME/HFE) electrolyte system.<sup>[72]</sup> The DFOB<sup>-</sup> derived low-solvation structure strongly influences the SEI formation and Li<sup>+</sup> reversibility and enables the Cu | NCM811 cells with high Li reversibility (99.34%).

The poor compatibility of PC-based electrolytes for LIBs with graphite anodes hinders their applications. As shown in Figure 8(e), the Cao's team induced PF<sub>6</sub><sup>-</sup> to construct an anion-induced-ion-solvent-coordinated (AI-ISC) weakly coordination structure to facilitate the PC-based electrolyte compatible with graphite | LiNi<sub>0.5</sub>Mn<sub>0.3</sub>Co<sub>0.2</sub>O<sub>2</sub> (NCM532) full battery by DEC co-solvent.<sup>[70]</sup> The pouch cell with the AI-ISC electrolyte delivers stable cycling performance with 91.5% retention after 750 cycles at the current density of 1 C in Figure 8(f).

### 5.2. Anion salts boosting flame retardant electrolytes

Tailoring non-flammable phosphate electrolytes with high safety and good Li reversibility are urgent requirements for practical LIBs. Anion-derived fluorine SEI layer can overcome the disadvantage of poor passivation ability of the flame-retardant solvents, thus enabling its application in LIBs. For example, trimethyl phosphate (TMP<sub>a</sub>) is an effective flame-retardant. However, it is generally regarded as an unqualified material due to its tendency to cause graphite exfoliation and battery failure in graphite-based LIBs. The unique solvation structure of TMP<sub>a</sub> in the LHCEs system and the composition of solvation sheath are adjusted by electrolyte additives, and an excellent LiFSI-TMP<sub>a</sub> based electrolyte with excellent electro-

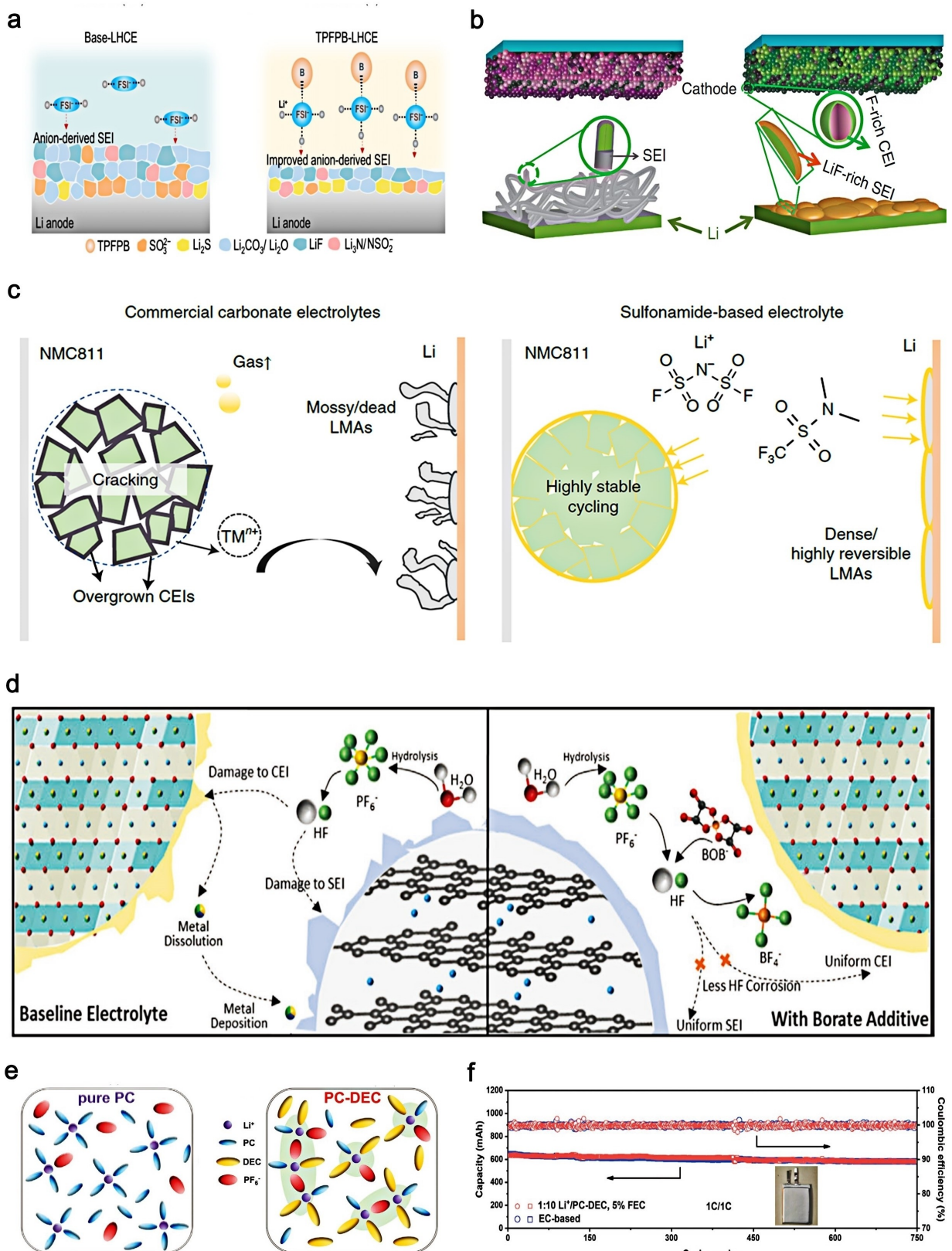


**Figure 8.** a) Schematic diagram of the electrolyte structure of  $\text{FSI}^-$  and the correspondingly formed SEI in Base-LHCEs and TPFPB-LHCEs. Reproduced with permission from Ref. [66]. Copyright (2021) Wiley-VCH. b) Variation of SEI and CEI chemistries formed in traditional carbonate and all-fluorinated electrolytes. Reproduced with permission from Ref. [67]. Copyright (2018) Springer Nature. c) Challenges for durable high-voltage  $\text{Li} \mid \text{NMC811}$  cells. Reproduced with permission from Ref. [68]. Copyright (2021) Springer Nature. d) Schematic of the enhanced cell performance for borate additive electrolyte in high-voltage full cell system. Reproduced with permission from Ref. [69]. Copyright (2022) Wiley-VCH. e) Schematic diagrams of the solvation structure of pure PC electrolyte and PC-DEC electrolyte. f) Cycling performance of the pouch cells at the rate of 1 C between the voltage of 3–4.2 V. Reproduced with permission from Ref. [70]. Copyright (2021) Wiley-VCH.

chemical performance in graphite||NCM811 batteries can be obtained.<sup>[73]</sup> Meanwhile, due to the flame retardant effect of  $\text{TMP}_\alpha$ , the flammability of the  $\text{TMP}_\alpha$ -based LHCEs system is meaningfully lower than that of conventional  $\text{LiPF}_6$ -organic carbonated electrolytes in Figure 9(a). In addition, Lu et al. designed a novel and sustainable dual-layer crystalline/polymeric SEI layer derived from LiDFOB-based phosphate/ether flame retardant electrolyte to achieve low self-extinguishing time and high Li reversibility in Figure 9(b).<sup>[74]</sup>

A flame-retardant LHCEs system inherits the advantages of the HCEs system, such as non-flammability and wide electro-

chemical stability window, and significantly overcomes the high viscosity, high cost, and poor wettability of the HCEs system. Zhang et al. proposed a flame retardant LHCEs system composed of 1.2 M LiFSI and flame-retardant TEP mixture LIBs in Figure 9(c and d).<sup>[75]</sup> However, their compatibility with electrode materials, especially graphite anodes, is still an obstacle due to the solid catalytic activity of the anode surface. Zhang et al. reported a method to improve the stability of non-flammable TEP electrolytes by regulating the ratio of Li salt to solvent in Figure 9(e).<sup>[76]</sup> At a higher Li salt-solvent molar ratio (1:2 LiFSI-TEP), most phosphate solvent molecules are coordi-

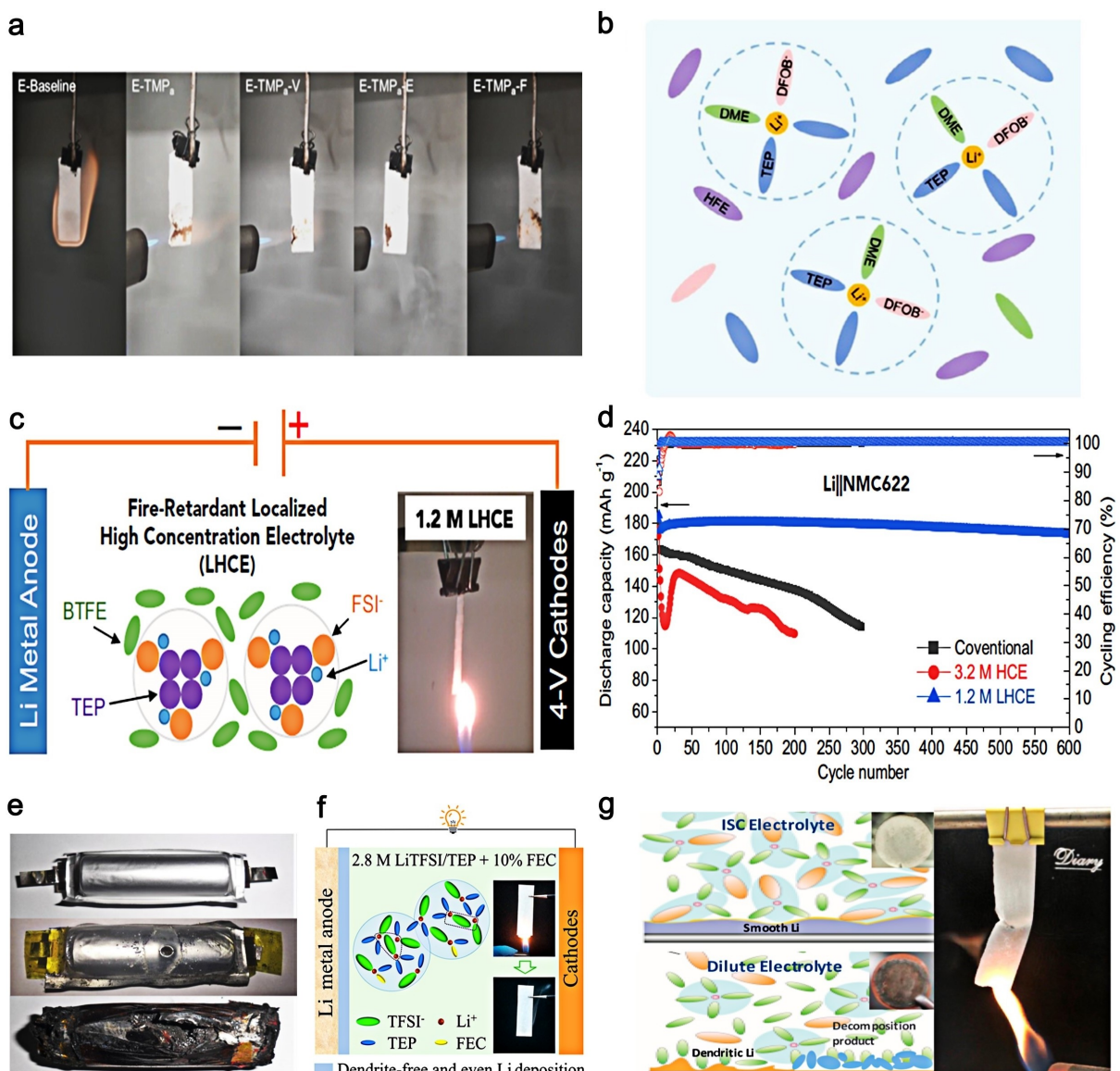


**Figure 9.** a) Flammability of various electrolytes determined by ignition test. Reproduced with permission from Ref. [73]. Copyright (2021) Wiley-VCH. b) Schemes of solvation structure of E-3 electrolyte (1.75 M LiDFOB in TEP/DME/HFE, 4:1:5 vol) and as-formed crystalline/polymeric dual-layer SEI. Reproduced with permission from Ref. [74]. Copyright (2021) Elsevier B.V. c) Schematic illustration for dilution by BTFE of an HCE consisting of 3.2 M LiFSI/TEP to form LHCEs, ignition tests, and d) corresponding electrochemical behavior of Li/NMC622 batteries. Reproduced with permission from Ref. [75]. Copyright (2018) Elsevier B.V. e) Nail penetration test for 18650 cells using 1:2 LiFSI-TEP + FEC-LiBOB electrolyte (middle) and commercial carbonate electrolyte (1.0 M LiPF<sub>6</sub>/EC:DEC:EMC = 1:1:1 by volume) (bottom). Reproduced with permission from Ref. [76]. Copyright (2018) Springer Nature. f) Schematic illustration of the representative environment of Li<sup>+</sup> in the diluted and concentrated electrolytes. Reproduced with permission from Ref. [77]. Copyright (2019) American Chemical Society. g) Schematic illustrations of the Li metal plating on a Cu electrode in low MR and high MR (ISC) electrolytes, and ignition tests. Reproduced with permission from Ref. [78]. Copyright (2019) American Chemical Society.

nated with  $\text{Li}^+$ , which can effectively suppress the adverse reaction of solvent molecules to the graphite anode.

Zhang et al. reported a flame-retardant electrolyte consisting of 2.8 M LiTFSI in TEP with 10 vol.% FEC as a high-performance electrolyte in Figure 9(f).<sup>[77]</sup> This system has almost no free solvent molecules and anions, which can reduce the reactivity of the electrolyte to the Li metal anode. Furthermore, the presence of FEC in the TEP-based electrolyte facilitates the formation of a stable LiF-rich SEI layer.

Liu et al. investigated the reduction stability of a wide range of non-flammable electrolyte salt and solvent ratios, demonstrating that the ionic solvent-coordinated (ISC) non-flammable LiFSI-TEP electrolyte enables dendrite-free Li metal plating/stripping copper electrodes with a high CE of 99.3% for up to 350 cycles in Figure 9(g).<sup>[78]</sup>

In Summary, this section provides new insights into the interrelationships of different anions in regulating the solvation sheath of lithium ions, which is instructive for the rational design of stable and safe electrolytes. The preferential decomposition products of solvents and anions in the solvating sheath are the main components of SEI. Tuning the composition and structure of  $\text{Li}^+$  solvation sheaths provides an efficient route to construct a uniform and stable SEI. In addition, with the increase in Li salt concentration, its solvation structure also changes significantly. A further in-depth understanding of the interaction of different types of anions in the solvation sheath will open new adventures for stable and safe lithium metal batteries to modulate the solvation sheath of  $\text{Li}^+$ .

## 6. Advanced Characterization and Measurement on Low Solvation Electrolytes

### 6.1. Potentiometric measurement

The solvation reactions of  $\text{Li}^+$  have been investigated using various spectroscopic techniques. Although these methods provide rich spectroscopic information on the localized binding structure, quantitative comparisons among many electrolytes remain a challenge. Finding a relevant single metric across the broad spectrum of electrolytes is a complex problem. In addition, analysis often involves complex deconvolution and spectral interpretation, which are not standardized across methods. And the presence of the same functional group in different solvents in mixed solvent systems adds to the challenge of single, quantifiable metrics, which are desirable to facilitate direct comparison of the solvation properties of different electrolyte formulations.

Cui et al. proposed a novel potentiometric method to research the  $\text{Li}^+$  solvation degree in LIBs electrolytes in Figure 10(a and b).<sup>[79]</sup> The open circuit potential was measured to the  $\text{Li}^+$  solvation energy relative to the reference electrolyte in galvanic cells with symmetrical electrodes but asymmetric electrolytes. The technique is quantitative and applicable to a wide range of formulations, which enables the cell potential of asymmetric electrolyte batteries as an indicator for characteriz-

ing electrolytes. Cui et al. established a tight correlation between cell potential and cyclability of electrolytes and then derived those solvents with more negative cell potentials, positive solvation energies, and weak binding energy to  $\text{Li}^+$ , leading to enhanced cyclability. Figure 10(c-h) shows these representative electrolyte solvents measured by open-circuit cell potential and CE. By plotting  $E_{\text{cell}}$  and CE, a clear negative correlation is found that solvents with more negative potential and positive solvation energy exhibit better cycling performance.

### 6.2. Small-angle X-ray scattering

A fundamental understanding of liquid electrolyte nanostructures promises to contribute to transformative gains in electrochemical energy storage capabilities. However, the solvation structure and molecular dynamics in electrolytes are difficult to probe, which limits the further improvement of macroscopic properties such as ionic conductivity, viscosity, and stability. Small-angle X-ray scattering (SAXS) is a non-destructive method for characterizing liquid nanostructures that provides unique insights into molecular clusters, anion-cation pairs, solvated sheaths, osmotic networks, aggregates, and domain sizes of electrolytes perspective, as shown in Figure 11(a). Notably, the SAXS method has a good temporal resolution, enabling the study of the operational characterization of molecular dynamics.<sup>[80]</sup> The unique capabilities of X-ray scattering for intramolecular and intermolecular relationships and the characterization of electrolyte nanostructures are highlighted.

The idea of using a non-solvent to dilute concentrated electrolytes was first proposed by Dokko et al. in 2013.<sup>[81]</sup> A hydrofluoroether solvent, HFE, was mixed with an equimolar glyme-Li salt complex. The results show that HFE does not disrupt the solvated structure of the glyme Li salt complex, but inhibits the dissolution of polysulfides in the electrolyte of Li-S batteries. Cuisinier et al.<sup>[82]</sup> designed a new AN and LiTFSI with HFE electrolyte in which all AN molecules are efficiently bound to  $\text{Li}^+$  to form a 2:1 complex, and HFE acts as a diluting solvent to reduce viscosity. The electrolyte has low volatility and minimal solubility for lithium polysulfides and is stable to Li metal anode. In addition, Umebayashi et al.<sup>[83]</sup> applied Raman spectroscopy, small X-ray total scattering experiments (HEXTS), and DFT calculations to clarify the  $\text{Li}^+$  local structure in the HFE diluted electrolyte. Powder diffraction file (PDF) analysis of total scattering is an inverse Fourier transform of simplified experimental data, which favors large  $q$  regions, especially high  $q$  parts. Although there are some differences in experimental setup and data analysis between the total X-ray scattering method and the SAXS method, the structure factors of liquids extracted from the same  $q$ -region should be the same for both methods. Their study confirms that HFE never directly coordinates with  $\text{Li}^+$ . In pure glyme-Li complexes, there are two types of CIPs, in which the anion complexes with  $\text{Li}^+$  are monodentate and bidentate. As the HFE is diluted, the Raman results show that the monodentate CIP decreased while the bidentate CIP remained unchanged. Meanwhile, a new peak

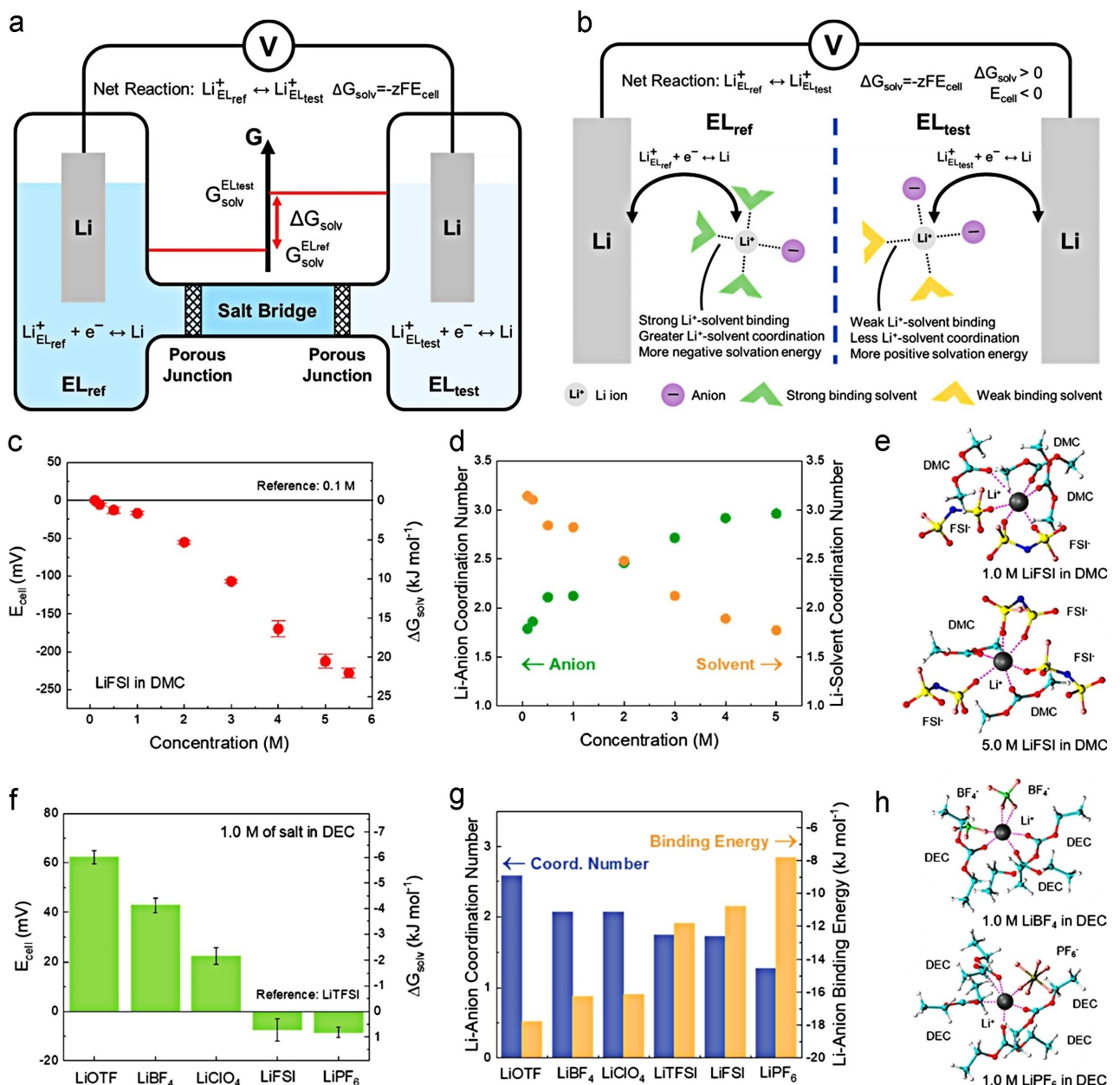


**Figure 10.** a) Experimental setup has two half-cells, each with lithium metal as electrode material and two different electrolytes. b) Model experiment illustrating the relationship between solvation energy and structure. c) Measured cell potentials at different concentrations of LiFSI in DMC. d) MD simulation results on the coordination number showing that coordination with solvent is weakened and coordination with anion is more pronounced as concentration increases. e) Simulated solvation structures at concentrations of 1.0 and 5.0 M LiFSI in DMC. f) Measured cell potentials of various salts of 1.0 M concentration in DEC. g) MD simulation results of Li-anion binding energy and coordination numbers. h) Simulated solvation structures of 1.0 M LiBF<sub>4</sub> in DEC and 1.0 M LiPF<sub>6</sub> in DEC. Reproduced with permission from Ref. [79]. Copyright (2021) American Chemical Society.

appears around 0.6–0.7 Å<sup>-1</sup> for the X-ray structure factor, as shown in Figure 11(b and c), indicating that the correlation between the ion pairs is more extended.

### 6.3. Nuclear magnetic resonance (NMR)

To reveal the solvation behavior in the mixed carbonate/ether electrolyte system, the NMR spectroscopy is performed using natural abundance <sup>17</sup>O NMR. In <sup>17</sup>O NMR spectroscopy, subtle

changes in the solvated sheath can directly affect the electronic environment of various intramolecular <sup>17</sup>O nuclei, which can be expressed as chemical shifts. Figure 12(a) illustrates the change of <sup>17</sup>O species after the addition of Li salts (LiTFSI and LiNO<sub>3</sub>) in pure DOL/DME solvent at room temperature.<sup>[44]</sup> The <sup>17</sup>O chemical shift of DME ( $\Delta = 3.6$  ppm) is larger than that of DOL ( $\Delta = 0.3$  ppm), indicating that Li<sup>+</sup> preferentially coordinates with DME rather than DOL. At room temperature, adding 10 vol.% FEC in ether solvent does not change the strong binding of DME to Li<sup>+</sup>. At  $-40^{\circ}\text{C}$ , all <sup>17</sup>O NMR peaks are

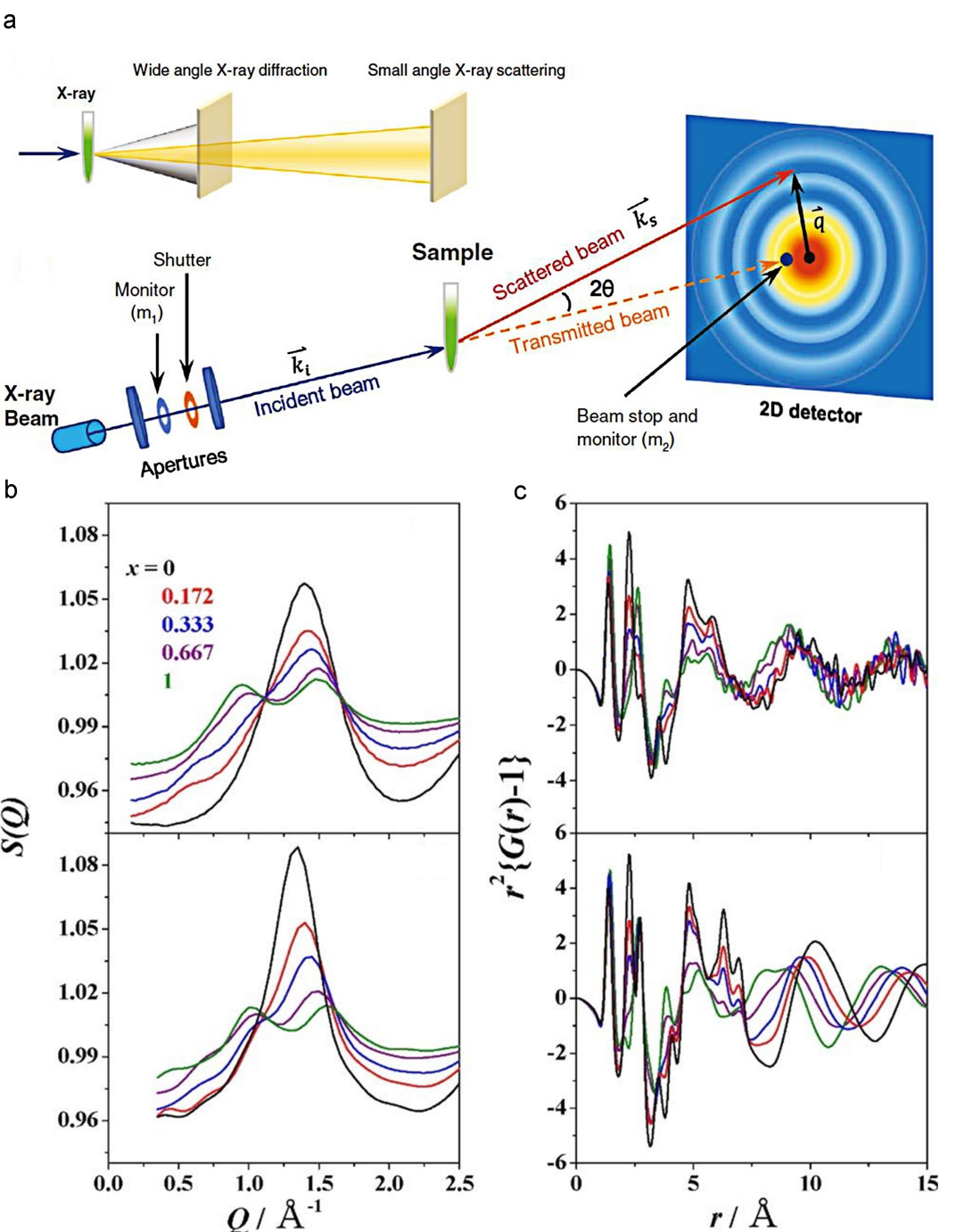


**Figure 11.** a) The difference between small and wide angle X-ray scattering, and small-angle X-ray diffraction setup of the synchrotron beamline at the Advanced Photon Source. Reproduced with permission from Ref. [80]. Copyright (2021) Wiley-VCH. b) Experimental X-ray structure factors at the  $Q$  range  $0-2.5 \text{\AA}^{-1}$  and corresponding MD and c) radial distribution functions as a form of at the  $r$  range  $0-15 \text{\AA}$  and corresponding MD for neat and HFE diluted  $[\text{Li}(\text{G4})]\text{[TFSA]}$  solvate ionic liquid at 298 K. Reproduced with permission from Ref. [83]. Copyright (2016) American Chemical Society.

broadened (i.e., the change in linewidth is greater than  $27^\circ\text{C}$ ) after adding Li salt, probably due to the rapid quadrupole relaxation in Figure 12(b). This is because that molecular redirection slows down at lower temperatures, while the anisotropic quadrupole interaction of  $^{17}\text{O}$  averaged at higher temperatures is now more pronounced. After Li salt addition at  $-40^\circ\text{C}$ , the DME peak is broadened to the baseline, indicating a significant synergy with  $\text{Li}^+$ . Substantial linewidth increases in

FEC peaks (115% for FEC-a and 49% for FEC-b compared to 31% for DOL) and peak shifts (0.7 ppm for FEC-a and 1.2 ppm for FEC-b compared to 31% for DOL only 0.3 ppm) indicate that FEC also has strong coordination with  $\text{Li}^+$  at  $-40^\circ\text{C}$ .

Bao et al. investigated the solvation reaction of  $\text{Li}^+$  in 1 M LiFSI/6FDMH-DME electrolyte in Figure 12(c).<sup>[56]</sup> The formulation of 1 M LiFSI/6FDMH-DME is similar to the recently developed LHCEs, but the solvation mechanism is different. In LHCEs,

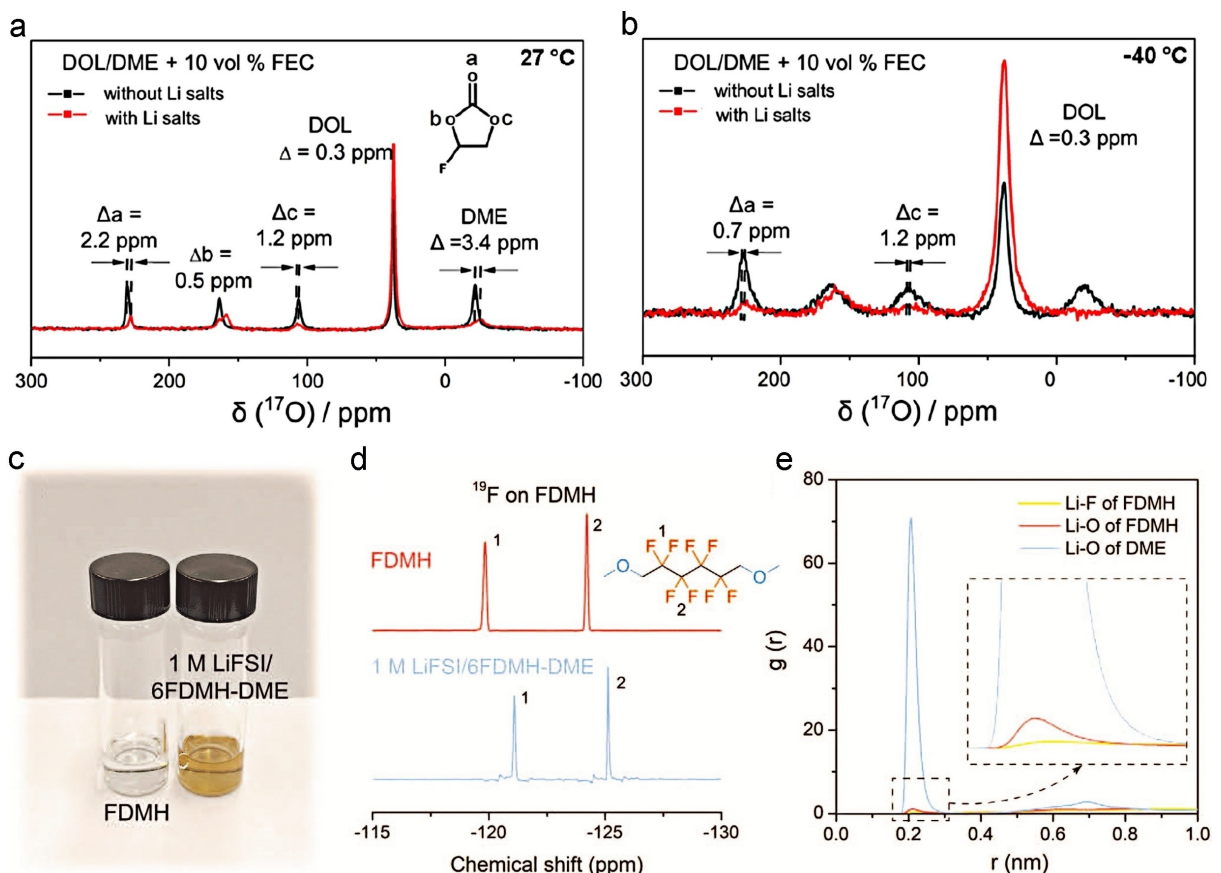


**Figure 12.** <sup>17</sup>O NMR spectra of FEC-modified ether electrolyte without (black) and with (red) the Li salts (LiTFSI and LiNO<sub>3</sub>) at a) 27 °C and b) -40 °C. Reproduced with permission from Ref. [44]. Copyright (2020) American Chemical Society. c) Digital photo of pure FDMH and 1 M LiFSI/6FDMH-DME electrolyte. d) <sup>19</sup>F NMR of FDMH and 1 M LiFSI/6FDMH-DME. e) Radial distribution functions of FDMH and DME molecules around Li-ions in the 1 M LiFSI/6FDMH-DME electrolyte. Reproduced with permission from Ref. [56]. Copyright (2021) Wiley-VCH.

fluorinated molecules act as diluents and do not participate in the solvation of Li<sup>+</sup>. In contrast, both FDMH and DME are involved in Li<sup>+</sup> solvation in 1 M LiFSI/6FDMH-DME electrolyte. Compared with pure FDMH, the <sup>19</sup>F NMR peak in 1 M LiFSI/6FDMH-DME electrolyte shows a clear front-field shift (Figure 12c), further verifying the interaction between F<sub>FDMH</sub><sup>-</sup> and Li<sup>+</sup>. When FDMH interacts with Li<sup>+</sup> and participates in the solvated sheath, the surrounding FSI<sup>-</sup> anions that are originally in the solvated structure can shield the FDMH molecule, resulting in a field advance of <sup>19</sup>F for the FDMH molecule. Meanwhile, atomistic MD is used to simulate the solvation environment in 1 M LiFSI/6FDMH-DME electrolyte in Figure 12(e). The radial distribution function verifies that lithium ions are not only solvated by DME molecules, but also by O<sub>FDMH</sub><sup>-</sup> and F<sub>FDMH</sub><sup>-</sup> solvents in the first solvation shell.

#### 6.4. Raman spectroscopy and Fourier transform infrared spectroscopy (FT-IR)

Raman technology has been widely used in studying the solvation and ion conduction mechanism of Li salts, allowing a good identification of factors affecting the performance of carbonated electrolytes. Liu et al. provided a method in which

the solvated structure of Li<sup>+</sup> in the electrolyte was found to be very important for the reversibility and electroplating behavior of Li metal at low temperatures. This study sets the performance bar for the operation of ultra-low temperature batteries and reveals key electrolyte design strategies to achieve this at the molecular level. The Raman spectra of the electrolyte and its components provide the experimental basis for the above results. These spectra are shown in Figure 13(a-c), where 1 M LiFSI DOL/DME and 1 M LiFSI DEE are compared with individual LiFSI salts, DME, DOL, and DEE solvents. It is known that upon dissolution, the anion-related peaks undergo a significant red shift due to the decreased coordination between the cation and anion and the increased coordination between the cation and the solvent. As shown in the LiFSI spectrum, when dissolved in DOL/DME solvent, the S-N-S bending peak of FSI<sup>-</sup> at 774 cm<sup>-1</sup> is significantly shifted to 720 cm<sup>-1</sup>, indicating a strong solution of the Li<sup>+/FSI<sup>-</sup> interaction separation, which is consistent with the solvated structure of SSIP. In contrast, the shift of the FSI<sup>-</sup> S-N-S bending peak in 1 M LiFSI DEE is much smaller, from 774 cm<sup>-1</sup> in pure salt to 748 cm<sup>-1</sup> in the electrolyte, indicating a much stronger Li<sup>+/FSI<sup>-</sup> interaction, which is the result of the CIP structure feature. These changes can also be found in FT-IR in Figure 13(d and e), where the C-O-C peak of DEE (1130 cm<sup>-1</sup>) undergoes a reduced shift compared to</sup></sup>

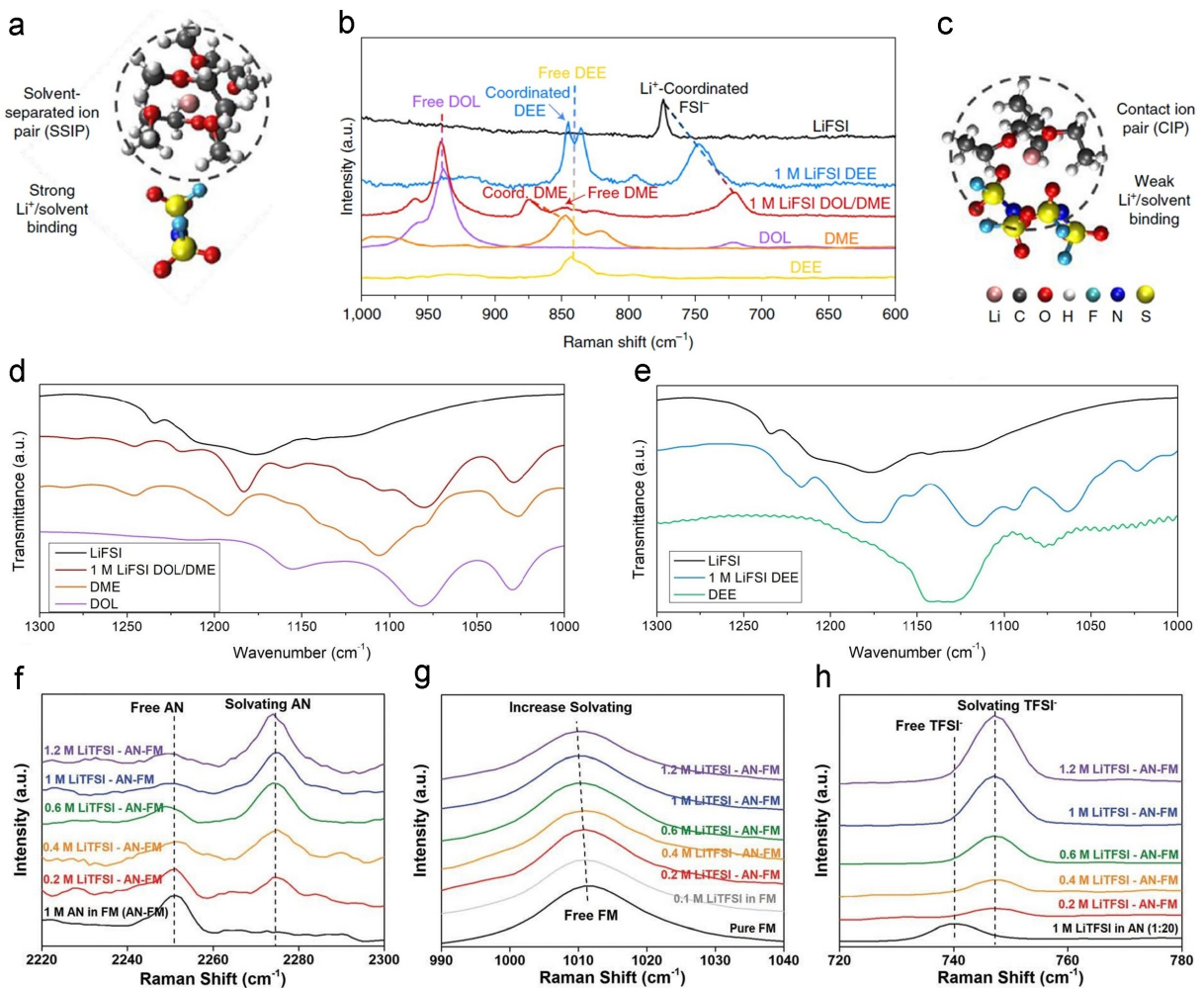


**Figure 13.** a) Most probable solvation structure extracted from MD simulation of 1 M LiFSI DOL/DME. b) Raman spectra obtained from electrolytes of interest and their components. c) Most probable solvation structure extracted from MD simulations of 1 M LiFSI DEE. d and e) FT-IR spectra of 1 M LiFSI electrolytes and their components. Reproduced with permission from Ref. [51]. Copyright (2021) Springer Nature. Solvation structure of bulk electrolyte Raman spectra of liquefied gas electrolytes with 1 M AN and increasing LiTFSI concentrations in f) 2220–2300 cm<sup>-1</sup> (C–N stretching vibration of AN molecules), g) 990–1040 cm<sup>-1</sup> (C–F stretching vibration of FM molecules), and h) 720–780 cm<sup>-1</sup> (S–N–S bending vibration of TFSI<sup>-</sup>). Reproduced with permission from Ref. [49]. Copyright (2020) The Royal Society of Chemistry.

DME (1106 cm<sup>-1</sup>) after the introduction of 1 M LiFSI. Furthermore, it is worth noting that the CIP solvation structure displayed by the DEE system may be responsible for the enhanced oxidative stability.

Meng et al. proposed a fluoromethane-based liquefied gas electrolyte with AN co-solvent and a higher salt concentration. The solvation structure of the liquefied gas electrolyte was studied by Raman spectroscopy. To determine the coordination of Li<sup>+</sup> to AN and FM molecules, Raman spectra of 1 M AN co-solvent were obtained in FM with different LiTFSI concentrations. The normalized intensity of the peak at 2252 cm<sup>-1</sup> gradually decreases with salt addition increasing, while a different peak appears at 2270 cm<sup>-1</sup> in Figure 13(f). At a salt concentration above 1 M, the strong coordination can be found between ammonium nitride and Li<sup>+</sup> and almost no free ammonium nitride can improve the oxidation stability of ammonium nitride and stabilize its interface with Li metal. The interaction of Li<sup>+</sup> and FM is also detected in Figure 13(g).

Although LiTFSI has low solubility in FM (< 0.1 M), red shift appears in the stretching peak of C–F (about 1012 cm<sup>-1</sup>) after adding 0.1 M LiTFSI in pure FM, indicating that with the lone electron pair of fluorine and the coordination of Li<sup>+</sup>, the bond order of C–F is disrupted. After this, Figure 13(h) shows that most TFSI<sup>-</sup> exist as free anions in the diluted LiTFSI-AN (1:20), while the TFSI<sup>-</sup> participates in aggregation in LiTFSI-AN-FM electrolyte due to the high salt-co-solvent ratio.

## 7. Conclusion and Perspective

In conclusion, the solvation structure of electrolytes is of crucial significance in determining the formation of SEI and CEI interfaces and further affecting the overall battery performance. With the desired direction to high-energy-density, super long lifespan, and extreme-condition batteries, the strategies for constructing the solvation structure of electrolytes should be

paid extraordinary attention to. In this review, we systematically summarize the regulation factors on the current solvation structure of electrolytes related to SEI and CEI layers issues. Four primary behaviors in LIBs electrolytes involving specific binding energy, solvation and de-solvation process, the diverse structure of solvents, and selection of Li salts are identified to play preponderant roles in determining the interfacial composition.

According to the previous research on electrolytes, different catastrophic issues existing in LIBs system are closely concerned with solvent molecules sheath, which can result in various decomposition compositions. In particular, the dehydrogenation reaction of the solvent accelerates the degradation of LIBs. We are delighted to smell an auspicious development path: revisiting the influencing factors of the solvation structure by determining the adsorption energies, activation energies, solvation/de-solvation processes, locations of the solvation sheath, and improving Li salts and novel solvents for rechargeable batteries. This provides new ideas and prospects for the development and application of electrolytes undoubtedly. We should pay attention to the adsorption energy, activation energy, and solvation/de-solvation process in the electrolyte, and further explore and solve the long-term thorny problem of electrolyte/electrode interphases failure.

Despite the fruitful results of the above studies, the mysteries of the solvation structures of electrolytes are still lacking due to the heterogeneous formation of complex interfaces, multi-step reductions, and mysterious ion transfer behaviors within the interfaces.<sup>[84]</sup> Therefore, a more comprehensive devotion is strongly advocated to promote a more thorough and complete understanding. Of particular note are the following vital aspects in future research.

- 1) Establishing precise correlations between specific binding energies and solvated coordination structures needs to be solved urgently. The too high or too low binding energy of  $\text{Li}^+$  and coordinated solvents will affect the dissociation and dissolution of solvated structures. Hence, establishing a consistent binding energy criterion needs to be explored and summarized in the future.
- 2) The more profound understanding of the  $\text{Li}^+$  transfer process at the SEI, CEI interfaces, and electrodes, including *in situ* microscopic visualization modes of the  $\text{Li}^+$  solvation/de-solvation process, has not been implemented. Therefore, finding factors affecting the solvation structure of electrolytes, exploring the de-solvation behavior of  $\text{Li}^+$ , and contriving advanced characterization techniques are expected to break through the bottleneck of the solvation structure of electrolytes to improve electrode/electrolyte interphases.
- 3) The solvation structure of the electrolyte should be thoroughly designed, taking into account the interfacial stability, binding energy, activation energy of solvation/de-solvation process, diverse structure, and intrinsic chemical interaction of solvents, and diversity of cations and anions.
- 4) Combining the aforementioned factors, it is expected to design a unified Li salt and solvent composition and establish a comprehensive electrolyte with a specific

solvated structure, which can satisfy the needs of most anodes, cathodes, and practical work, and effectively avoid complex products and production lines and excess capacity.

To effectively solve the aforementioned aspects, the joint efforts of physics, chemistry, materials science, and other disciplines are required to provide profound theoretical and experimental insights. It is believed that with continuous cooperation and investment, there will be more remarkable breakthroughs in the understanding of the solvated structure of electrolytes, which will indeed promote the tremendous success of existing LIBs and other battery chemical products.

## Acknowledgements

This research is supported by the Science Foundation of National Key Laboratory of Science and Technology on Advanced Composites in Special Environments, and the National Natural Science Foundation of China (12002109).

## Conflict of Interest

The authors declare no conflict of interest.

- [1] a) G. M. Hobold, J. Lopez, R. Guo, N. Minafra, A. Banerjee, Y. S. Meng, Y. Shao-Horn, B. M. Gallant, *Nat. Energy* **2021**, *6*, 951–960; b) Y. Yamada, J. H. Wang, S. Ko, E. Watanabe, A. Yamada, *Nat. Energy* **2019**, *4*, 269–280; c) F. Liu, R. Xu, Y. C. Wu, D. T. Boyle, A. K. Yang, J. W. Xu, Y. Y. Zhu, Y. S. Ye, Z. A. Yu, Z. W. Zhang, X. Xiao, W. X. Huang, H. S. Wang, H. Chen, Y. Cui, *Nature* **2021**, *600*, 659–663; d) S. Y. Hou, X. Ji, K. Gaskell, P. F. Wang, L. N. Wang, J. J. Xu, R. M. Sun, O. Borodin, C. S. Wang, *Science* **2021**, *374*, 172–178; e) L. W. Dong, Y. P. Liu, K. C. Wen, D. J. Chen, D. W. Rao, J. P. Liu, B. T. Yuan, Y. F. Dong, Z. Wu, Y. F. Liang, M. Q. Yang, J. Y. Ma, C. H. Yang, C. Xia, B. Y. Xia, J. C. Han, G. M. Wang, Z. P. Guo, W. D. He, *Adv. Sci.* **2021**, *9*, 2104699; f) L. W. Dong, Y. P. Liu, D. J. Chen, Y. P. Han, Y. P. Ji, J. P. Liu, B. T. Yuan, Y. F. Dong, Q. Li, S. Y. Zhou, S. J. Zhong, Y. F. Liang, M. Q. Yang, C. H. Yang, W. D. He, *Energy Storage Mater.* **2022**, *44*, 527–536.
- [2] a) M. Born, *Zeitschrift für Physik* **1920**, *1*, 45–48; b) L. Onsager, *J. Am. Chem. Soc.* **1936**, *58*, 1486–1493; c) H. S. Frank, *J. Am. Chem. Soc.* **1941**, *63*, 1789–1799; d) H. S. Frank, M. W. Evans, *J. Chem. Phys.* **1945**, *13*, 507–532; e) R. H. Stokes, R. A. Robinson, *J. Am. Chem. Soc.* **1948**, *70*, 1870; f) B. G. Cox, A. J. Parker, W. E. Waghorne, *J. Phys. Chem.* **1974**, *78*, 1731–1740; g) J. C. Ghosh, *J. Chem. Soc. Trans.* **1918**, *113*, 449–458.
- [3] M. S. Whittingham, *Science* **1976**, *192*, 1126–1127.
- [4] R. Fong, U. Vonsacken, J. R. Dahn, *J. Electrochem. Soc.* **1990**, *137*, 2009–2013.
- [5] M. S. Whittingham, *Proc. IEEE* **2012**, *100*, 1518–1534.
- [6] X. L. Fan, C. S. Wang, *Chem. Soc. Rev.* **2021**, *50*, 10486–10566.
- [7] a) Y. L. Jie, X. D. Ren, R. G. Cao, W. B. Cai, S. H. Jiao, *Adv. Funct. Mater.* **2020**, *30*, 23; b) Z. S. Wang, H. P. Wang, S. A. Qi, D. X. Wu, J. D. Huang, X. Li, C. Y. Wang, J. M. Ma, *EcoMat* **2022**, *4*, e12200.
- [8] a) J. G. Zhang, W. Xu, J. Xiao, X. Cao, J. Liu, *Chem. Rev.* **2020**, *120*, 13312–13348; b) X. Cao, X. D. Ren, L. F. Zou, M. H. Engelhard, W. Huang, H. S. Wang, B. E. Matthews, H. Lee, C. J. Niu, B. W. Arey, Y. Cui, C. M. Wang, J. Xiao, J. Liu, W. Xu, J. G. Zhang, *Nat. Energy* **2019**, *4*, 796–805; c) J. T. Hu, Y. C. Ji, G. R. Zheng, W. Y. Huang, Y. Lin, L. Y. Yang, F. Pan, *Aggregate* **2022**, *3*, 21; d) S. Y. Yuan, T. Y. Kong, Y. Y. Zhang, P. Dong, Y. J. Zhang, X. L. Dong, Y. G. Wang, Y. Y. Xia, *Angew. Chem. Int. Ed.* **2021**, *60*, 25624–25638; e) H. R. Cheng, Q. J. Sun, L. L. Li, Y. G. Zou, Y. Q. Wang, T. Cai, F. Zhao, G. Liu, Z. Ma, W. Wahyudi, Q. Li, J. Ming, *ACS Energy Lett.* **2022**, *7*, 490–513.
- [9] Q. Pang, A. Shyamsunder, B. Narayanan, C. Y. Kwok, L. A. Curtiss, L. F. Nazar, *Nat. Energy* **2018**, *3*, 783–791.

- [10] M. Okoshi, Y. Yamada, S. Komaba, A. Yamada, H. Nakai, *J. Electrochem. Soc.* **2017**, *164*, A54–A60.
- [11] a) Q. Y. Li, D. P. Lu, J. M. Zheng, S. H. Jiao, L. L. Luo, C. M. Wang, K. Xu, J. G. Zhang, W. Xu, *ACS Appl. Mater. Interfaces* **2017**, *9*, 42761–42768; b) Z. Fang, Y. Yang, T. L. Zheng, N. Wang, C. X. Wang, X. L. Dong, Y. G. Wang, Y. Y. Xia, *Energy Storage Mater.* **2021**, *42*, 477–483; c) C. Yan, H. R. Li, X. Chen, X. Q. Zhang, X. B. Cheng, R. Xu, J. Q. Huang, Q. Zhang, *J. Am. Chem. Soc.* **2019**, *141*, 9422–9429.
- [12] a) L. D. Xing, X. W. Zheng, M. Schroeder, J. Alvarado, A. V. Cresce, K. Xu, Q. S. Li, W. S. Li, *Acc. Chem. Res.* **2018**, *51*, 282–289; b) J. Ming, Z. Cao, Y. Q. Wu, W. Wahyudi, W. X. Wang, X. R. Guo, L. Cavallo, J. Y. Hwang, A. Shamim, L. J. Li, Y. K. Sun, H. N. Alshareef, *ACS Energy Lett.* **2019**, *4*, 2613–2622.
- [13] X. Q. Zhang, X. Chen, L. P. Hou, B. Q. Li, X. B. Cheng, J. Q. Huang, Q. Zhang, *ACS Energy Lett.* **2019**, *4*, 411–416.
- [14] Z. Yu, N. P. Balsara, O. Borodin, A. A. Gewirth, N. T. Hahn, E. J. Maginn, K. A. Persson, V. Srinivasan, M. F. Toney, K. Xu, K. R. Zavadil, L. A. Curtiss, L. Cheng, *ACS Energy Lett.* **2022**, *7*, 461–470.
- [15] a) X. W. Yu, A. Manthiram, *Energy Environ. Sci.* **2018**, *11*, 527–543; b) B. Liao, H. Y. Li, M. Q. Xu, L. D. Xing, Y. H. Liao, X. B. Ren, W. Z. Fan, L. Yu, K. Xu, W. S. Li, *Adv. Energy Mater.* **2018**, *8*, 16; c) P. B. Zhai, L. X. Liu, X. K. Gu, T. S. Wang, Y. J. Gong, *Adv. Energy Mater.* **2020**, *10*, 32; d) G. X. Li, *Adv. Energy Mater.* **2021**, *11*, 14; e) C. Yan, R. Xu, Y. Xiao, J. F. Ding, L. Xu, B. Q. Li, J. Q. Huang, *Adv. Funct. Mater.* **2020**, *30*, 21.
- [16] a) N. Takenaka, A. Bouibes, Y. Yamada, M. Nagaoka, A. Yamada, *Adv. Mater.* **2021**, *33*, 15; b) Z. Chang, H. Yang, Y. Qiao, X. Zhu, P. He, H. Zhou, *Adv. Mater.* **2022**, e2201339.
- [17] M. S. Kim, Z. W. Zhang, P. E. Rudnicki, Z. A. Yu, J. Y. Wang, H. S. Wang, S. T. Oyakhire, Y. L. Chen, S. C. Kim, W. B. Zhang, D. T. Boyle, X. Kong, R. Xu, Z. J. Huang, W. Huang, S. F. Bent, L. W. Wang, J. Qin, Z. N. Bao, Y. Cui, *Nat. Mater.* **2022**, *21*, 445–454.
- [18] X. Chen, X. Q. Zhang, H. R. Li, Q. Zhang, *Batteries & Supercaps* **2019**, *2*, 128–131.
- [19] X. Chen, Q. Zhang, *Acc. Chem. Res.* **2020**, *53*, 1992–2002.
- [20] a) C. Yan, H. Yuan, H. S. Park, J. Q. Huang, *J. Energy Chem.* **2020**, *47*, 217–220; b) A. Gross, S. Sakong, *Curr. Opin. Electrochem.* **2019**, *14*, 1–6; c) P. C. Zou, Y. M. Sui, H. C. Zhan, C. Y. Wang, H. L. Xin, H. M. Cheng, F. Y. Kang, C. Yang, *Chem. Rev.* **2021**, *121*, 5986–6056.
- [21] H. P. Wu, H. Jia, C. M. Wang, J. G. Zhang, W. Xu, *Adv. Energy Mater.* **2021**, *11*, 35.
- [22] a) B. T. Yuan, K. C. Wen, D. J. Chen, Y. P. Liu, Y. F. Dong, C. Feng, Y. P. Han, J. C. Han, Y. Q. Zhang, C. Xia, A. Sun, W. D. He, *Adv. Funct. Mater.* **2021**, *31*, 49; b) S. J. Zhong, B. T. Yuan, Z. X. Guang, D. J. Chen, Q. Li, L. W. Dong, Y. P. Ji, Y. F. Dong, J. C. Han, W. D. He, *Energy Storage Mater.* **2021**, *41*, 805–841; c) R. Weber, M. Genovese, A. J. Louli, S. Hames, C. Martin, I. G. Hill, J. R. Dahn, *Nat. Energy* **2019**, *4*, 683–689.
- [23] a) C. P. Yang, Y. X. Yin, S. F. Zhang, N. W. Li, Y. G. Guo, *Nat. Commun.* **2015**, *6*, 9; b) X. Wang, W. Zeng, L. Hong, W. W. Xu, H. K. Yang, F. Wang, H. G. Duan, M. Tang, H. Q. Jiang, *Nat. Energy* **2018**, *3*, 227–235.
- [24] Y. X. Xie, Y. X. Huang, X. H. Wu, C. G. Shi, L. N. Wu, C. Song, J. J. Fan, P. Dai, L. Huang, Y. J. Hua, C. T. Wang, Y. M. Wei, S. G. Sun, *J. Mater. Chem. A* **2021**, *9*, 17317–17326.
- [25] J. F. Ding, R. Xu, N. Yao, X. Chen, Y. Xiao, Y. X. Yao, C. Yan, J. Xie, J. Q. Huang, *Angew. Chem. Int. Ed.* **2021**, *60*, 11442–11447.
- [26] C. Zhu, C. Sun, R. Li, S. Weng, L. Fan, X. Wang, L. Chen, M. Noked, X. Fan, *ACS Energy Lett.* **2022**, *7*, 1338–1347.
- [27] Y. X. Yao, X. Chen, C. Yan, X. Q. Zhang, W. L. Cai, J. Q. Huang, Q. Zhang, *Angew. Chem. Int. Ed.* **2021**, *60*, 4090–4097; *Angew. Chem.* **2021**, *133*, 4136–4143.
- [28] S. Y. Yuan, S. T. Weng, F. Wang, X. L. Dong, Y. G. Wang, Z. X. Wang, C. Shen, J. L. Bao, X. F. Wang, Y. Y. Xia, *Nano Energy* **2021**, *83*, 11.
- [29] C. Liao, L. F. Han, X. W. Mu, Y. L. Zhu, N. Wu, J. Y. Lu, Y. G. Zhao, X. J. Li, Y. Hu, Y. C. Kan, L. Song, *ACS Appl. Mater. Interfaces* **2021**, *13*, 46783–46793.
- [30] X. D. Ren, L. F. Zou, X. Cao, M. H. Engelhard, W. Liu, S. D. Burton, H. Lee, C. J. Niu, B. E. Matthews, Z. H. Zhu, C. M. Wang, B. W. Arey, J. Xiao, J. Liu, J. G. Zhang, W. Xu, *Joule* **2019**, *3*, 1662–1676.
- [31] J. Alvarado, M. A. Schroeder, T. P. Pollard, X. F. Wang, J. Z. Lee, M. H. Zhang, T. Wynn, M. Ding, O. Borodin, Y. S. Meng, K. Xu, *Energy Environ. Sci.* **2019**, *12*, 780–794.
- [32] W. Liu, J. X. Li, W. T. Li, H. Y. Xu, C. Zhang, X. P. Qiu, *Nat. Commun.* **2020**, *11*, 11.
- [33] X. R. Yang, M. Lin, G. R. Zheng, J. Wu, X. S. Wang, F. C. Ren, W. G. Zhang, Y. Liao, W. M. Zhao, Z. R. Zhang, N. B. Xu, W. L. Yang, Y. Yang, *Adv. Funct. Mater.* **2020**, *30*, 12.
- [34] H. H. Sun, J. D. Liu, J. He, H. P. Wang, G. X. Jiang, S. H. Qi, J. M. Ma, *Sci. Bull.* **2022**, *67*, 725–732.
- [35] X. Liu, X. Shen, L. Luo, F. Zhong, X. Ai, H. Yang, Y. Cao, *ACS Energy Lett.* **2021**, *4*, 4282–4290.
- [36] Z. Chang, Y. Qiao, H. Deng, H. J. Yang, P. He, H. S. Zhou, *Joule* **2020**, *4*, 1776–1789.
- [37] P. M. Chekushkin, I. S. Merenkov, V. S. Smirnov, S. A. Kislenko, V. A. Nikitina, *Electrochim. Acta* **2021**, *372*, 9.
- [38] Z. X. Wang, F. L. Qi, L. C. Yin, Y. Shi, C. G. Sun, B. G. An, H. M. Cheng, F. Li, *Adv. Energy Mater.* **2020**, *10*, 9.
- [39] R. Xu, C. Yan, Y. Xiao, M. Zhao, H. Yuan, J. Q. Huang, *Energy Storage Mater.* **2020**, *28*, 401–406.
- [40] Y. S. Li, Y. Qi, *Energy Environ. Sci.* **2019**, *12*, 1286–1295.
- [41] K. Xu, A. von Cresce, U. Lee, *Langmuir* **2010**, *26*, 11538–11543.
- [42] Y. G. Zou, Z. Cao, J. L. Zhang, W. Wahyudi, Y. Q. Wu, G. Liu, Q. Li, H. R. Cheng, D. Y. Zhang, G. T. Park, L. Cavallo, T. D. Anthopoulos, L. M. Wang, Y. K. Sun, J. Ming, *Adv. Mater.* **2021**, *33*, 12.
- [43] a) N. Zhang, T. Deng, S. Zhang, C. Wang, L. Chen, C. Wang, X. Fan, *Adv. Mater.* **2021**, e2107899; b) W. L. Cai, Y. X. Yao, G. L. Zhu, C. Yan, L. L. Jiang, C. X. He, J. Q. Huang, Q. Zhang, *Chem. Soc. Rev.* **2020**, *49*, 3806–3833.
- [44] A. C. Thenuwara, P. P. Shetty, N. Kondekar, S. E. Sandoval, K. Cavallaro, R. May, C. T. Yang, L. E. Marbella, Y. Qi, M. T. McDowell, *ACS Energy Lett.* **2020**, *5*, 2411–2420.
- [45] a) D. Luo, M. Li, Y. Zheng, Q. Y. Ma, R. Gao, Z. Zhang, H. Z. Dou, G. B. Wen, L. L. Shui, A. P. Yu, X. Wang, Z. W. Chen, *Adv. Sci.* **2021**, *8*, 20; b) J. Holoubek, K. Kim, Y. J. Yin, Z. H. Wu, H. D. Liu, M. Q. Li, A. Chen, H. P. Gao, G. R. Cai, T. A. Pascal, P. Liu, Z. Chen, *Energy Environ. Sci.* **2022**, *15*, 1647–1658.
- [46] a) J. Y. Wang, W. Huang, A. Pei, Y. Z. Li, F. F. Shi, X. Y. Yu, Y. Cui, *Nat. Energy* **2019**, *4*, 664–670; b) J. Holoubek, M. Y. Yu, S. C. Yu, M. Q. Li, Z. H. Wu, D. W. Xia, P. Bhaladhere, M. S. Gonzalez, T. A. Pascal, P. Liu, Z. Chen, *ACS Energy Lett.* **2020**, *5*, 1438–1447; c) A. Gupta, A. Manthiram, *Adv. Energy Mater.* **2020**, *10*, 14; d) X. D. Lin, G. D. Zhou, J. P. Liu, J. Yu, M. B. Effat, J. X. Wu, F. Ciucci, *Adv. Energy Mater.* **2020**, *10*, 28.
- [47] a) Y. Feng, L. M. Zhou, H. Ma, Z. H. Wu, Q. Zhao, H. X. Li, K. Zhang, J. Chen, *Energy Environ. Sci.* **2022**, *15*, 1711–1759; b) D. Hubble, D. E. Brown, Y. Z. Zhao, C. Fang, J. Lau, B. D. McCloskey, G. Liu, *Energy Environ. Sci.* **2022**, *15*, 550–578.
- [48] X. L. Dong, Y. X. Lin, P. L. Li, Y. Y. Ma, J. H. Huang, D. Bin, Y. G. Wang, Y. Qi, Y. Y. Xia, *Angew. Chem. Int. Ed.* **2019**, *58*, 5623–5627; *Angew. Chem.* **2019**, *131*, 5679–5683.
- [49] Y. Y. C. Yang, Y. J. Yin, D. M. Davies, M. H. Zhang, M. Mayer, Y. H. Zhang, E. S. Sablina, S. Wang, J. Z. Lee, O. Borodin, C. S. Rustomji, Y. S. Meng, *Energy Environ. Sci.* **2020**, *13*, 2209–2219.
- [50] X. L. Fan, X. Ji, L. Chen, J. Chen, T. Deng, F. D. Han, J. Yue, N. Piao, R. X. Wang, X. Q. Zhou, X. Z. Xiao, L. X. Chen, C. S. Wang, *Nat. Energy* **2019**, *4*, 882–890.
- [51] J. Holoubek, H. Liu, Z. Wu, Y. Yin, X. Xing, G. Cai, S. Yu, H. Zhou, T. A. Pascal, Z. Chen, P. Liu, *Nat. Energy* **2021**, *6*, 303–313.
- [52] Z. X. Wang, Z. H. Sun, Y. Shi, F. L. Qi, X. N. Gao, H. C. Yang, H. M. Cheng, F. Li, *Adv. Energy Mater.* **2021**, *11*, 9.
- [53] C. S. Rustomji, Y. Yang, T. K. Kim, J. Mac, Y. J. Kim, E. Caldwell, H. Chung, S. Meng, *Science* **2017**, *356*, 10.
- [54] J. Liu, Z. N. Bao, Y. Cui, E. J. Dufek, J. B. Goodenough, P. Khalifah, Q. Y. Li, B. Y. Liaw, P. Liu, A. Manthiram, Y. S. Meng, V. R. Subramanian, M. F. Toney, V. V. Viswanathan, M. S. Whittingham, J. Xiao, W. Xu, J. H. Yang, X. Q. Yang, J. G. Zhang, *Nat. Energy* **2019**, *4*, 180–186.
- [55] Z. Yu, P. E. Rudnicki, Z. W. Zhang, Z. J. Huang, H. Celik, S. T. Oyakhire, Y. L. Chen, X. Kong, S. C. Kim, X. Xiao, H. S. Wang, Y. Zheng, G. A. Kamat, M. S. Kim, S. F. Bent, J. Qin, Y. Cui, Z. N. Bao, *Nat. Energy* **2022**, *7*, 94–106.
- [56] H. S. Wang, Z. Yu, X. Kong, W. L. Huang, Z. W. Zhang, D. G. Mackanic, X. Y. Huang, J. Qin, Z. N. Bao, Y. Cui, *Adv. Mater.* **2021**, *33*, 9.
- [57] Z. Yu, H. S. Wang, X. Kong, W. Huang, Y. C. Tsao, D. G. Mackanic, K. C. Wang, X. C. Wang, W. X. Huang, S. Choudhury, Y. Zheng, C. V. Amanchukwu, S. T. Hung, Y. T. Ma, E. G. Lomeli, J. Qin, Y. Cui, Z. N. Bao, *Nat. Energy* **2020**, *5*, 526–533.
- [58] G. Zhang, X. Deng, J. Li, J. Wang, G. Shi, Y. Yang, J. Chang, K. Yu, S.-S. Chi, H. Wang, P. Wang, Z. Liu, Y. Gao, Z. Zheng, Y. Deng, C. Wang, *Nano Energy* **2022**, *95*, 107014.
- [59] W. D. Zhang, Q. Wu, J. X. Huang, L. Fan, Z. Y. Shen, Y. He, Q. Feng, G. N. Zhu, Y. Y. Lu, *Adv. Mater.* **2020**, *32*, 11.
- [60] Z. H. Piao, P. T. Xiao, R. P. Luo, J. B. Ma, R. H. Gao, C. Li, J. Y. Tan, K. Yu, G. M. Zhou, H. M. Cheng, *Adv. Mater.* **2022**, *34*, 10.

- [61] W. J. Xue, Z. Shi, M. J. Huang, S. T. Feng, C. Wang, F. Wang, J. Lopez, B. Qiao, G. Y. Xu, W. X. Zhang, Y. H. Dong, R. Gao, Y. Shao-Horn, J. A. Johnson, J. Li, *Energy Environ. Sci.* **2020**, *13*, 212–220.
- [62] J. M. Zheng, M. H. Engelhard, D. H. Mei, S. H. Jiao, B. J. Polzin, J. G. Zhang, W. Xu, *Nat. Energy* **2017**, *2*, 8.
- [63] S. Jurng, Z. L. Brown, J. Kim, B. L. Lucht, *Energy Environ. Sci.* **2018**, *11*, 2600–2608.
- [64] a) T. Li, X. Q. Zhang, P. Shi, Q. Zhang, *Joule* **2019**, *3*, 2647–2661; b) S. L. Zhang, Y. Liu, Q. N. Fan, C. F. Zhang, T. F. Zhou, K. Kalantar-Zadeh, Z. P. Guo, *Energy Environ. Sci.* **2021**, *14*, 4177–4202.
- [65] X. S. Wang, S. W. Wang, H. R. Wang, W. Q. Tu, Y. Zhao, S. Li, Q. Liu, J. R. Wu, Y. Z. Fu, C. P. Han, F. Y. Kang, B. H. Li, *Adv. Mater.* **2021**, *33*, 11.
- [66] T. Li, X. Q. Zhang, N. Yao, Y. X. Yao, L. P. Hou, X. Chen, M. Y. Zhou, J. Q. Huang, Q. Zhang, *Angew. Chem. Int. Ed.* **2021**, *60*, 22683–22687.
- [67] X. L. Fan, L. Chen, O. Borodin, X. Ji, J. Chen, S. Hou, T. Deng, J. Zheng, C. Y. Yang, S. C. Liou, K. Amine, K. Xu, C. S. Wang, *Nat. Nanotechnol.* **2018**, *13*, 715–722.
- [68] W. J. Xue, M. J. Huang, Y. T. Li, Y. G. Zhu, R. Gao, X. H. Xiao, W. X. Zhang, S. P. Li, G. Y. Xu, Y. Yu, P. Li, J. Lopez, D. W. Yu, Y. H. Dong, W. W. Fan, Z. Shi, R. Xiong, C. J. Sun, I. Hwang, W. K. Lee, Y. Shao-Horn, J. A. Johnson, J. Li, *Nat. Energy* **2021**, *6*, 495–505.
- [69] Y. X. Li, W. K. Li, R. Shimizu, D. Y. Cheng, H. N. Nguyen, J. Paulsen, S. Kumakura, M. H. Zhang, Y. S. Meng, *Adv. Energy Mater.* **2022**, *12*, 13.
- [70] X. W. Liu, X. H. Shen, H. Li, P. Li, L. B. Luo, H. M. Fan, X. M. Feng, W. H. Chen, X. P. Ai, H. X. Yang, Y. L. Cao, *Adv. Energy Mater.* **2021**, *11*, 9.
- [71] X. D. Ren, S. R. Chen, H. Lee, D. H. Mei, M. H. Engelhard, S. D. Burton, W. G. Zhao, J. M. Zheng, Q. Y. Li, M. S. Ding, M. Schroeder, J. Alvarado, K. Xu, Y. S. Meng, J. Liu, J. G. Zhang, W. Xu, *Chem* **2018**, *4*, 1877–1892.
- [72] S. Y. Li, Q. L. Liu, W. D. Zhang, L. Fan, X. Y. Wang, X. Wang, Z. Y. Shen, X. X. Zang, Y. Zhao, F. Y. Ma, Y. Y. Lu, *Adv. Sci.* **2021**, *8*, 10.
- [73] H. Jia, Y. B. Xu, X. H. Zhang, S. D. Burton, P. Y. Gao, B. E. Matthews, M. H. Engelhard, K. S. Han, L. R. Zhong, C. M. Wang, W. Xu, *Angew. Chem. Int. Ed.* **2021**, *60*, 12999–13006.
- [74] S. Y. Li, S. C. Zhang, S. Y. Chai, X. X. Zang, C. Cheng, F. Y. Ma, L. Zhang, Y. Y. Lu, *Energy Storage Mater.* **2021**, *42*, 628–635.
- [75] S. R. Chen, J. M. Zheng, L. Yu, X. D. Ren, M. H. Engelhard, C. J. Niu, H. Lee, W. Xu, J. Xiao, J. Liu, J. G. Zhang, *Joule* **2018**, *2*, 1548–1558.
- [76] Z. Q. Zeng, V. Murugesan, K. S. Han, X. Y. Jiang, Y. L. Cao, L. F. Xiao, X. P. Ai, H. X. Yang, J. G. Zhang, M. L. Sushko, J. Liu, *Nat. Energy* **2018**, *3*, 674–681.
- [77] Y. Dong, N. Zhang, C. X. Li, Y. F. Zhang, M. Jia, Y. Y. Wang, Y. R. Zhao, L. F. Jiao, F. Y. Cheng, J. Z. Xu, *ACS Appl. Energ. Mater.* **2019**, *2*, 2708–2716.
- [78] L. F. Xiao, Z. Q. Zeng, X. W. Liu, Y. J. Fang, X. Y. Jiang, Y. Y. Shao, L. Zhuang, X. P. Ai, H. X. Yang, Y. L. Cao, J. Liu, *ACS Energy Lett.* **2019**, *4*, 483–488.
- [79] S. C. Kim, X. Kong, R. A. Vila, W. Huang, Y. L. Chen, D. T. Boyle, Z. A. Yu, H. S. Wang, Z. N. Bao, J. Qin, Y. Cui, *J. Am. Chem. Soc.* **2021**, *143*, 10301–10308.
- [80] K. Qian, R. E. Winans, T. Li, *Adv. Energy Mater.* **2021**, *11*, 22.
- [81] K. Dokko, N. Tachikawa, K. Yamauchi, M. Tsuchiya, A. Yamazaki, E. Takashima, J. W. Park, K. Ueno, S. Seki, N. Serizawa, M. Watanabe, *J. Electrochem. Soc.* **2013**, *160*, A1304–A1310.
- [82] M. Cuisinier, P. E. Cabelguen, B. D. Adams, A. Garsuch, M. Balasubramanian, L. F. Nazar, *Energy Environ. Sci.* **2014**, *7*, 2697–2705.
- [83] S. Saito, H. Watanabe, K. Ueno, T. Mandai, S. Seki, S. Tsuzuki, Y. Kameda, K. Dokko, M. Watanabe, Y. Umebayashi, *J. Phys. Chem. B* **2016**, *120*, 3378–3387.
- [84] Y. W. Sun, T. Z. Yang, H. Q. Ji, J. Q. Zhou, Z. K. Wang, T. Qian, C. L. Yan, *Adv. Energy Mater.* **2020**, *10*, 16.

Manuscript received: June 7, 2022

Revised manuscript received: August 9, 2022

Accepted manuscript online: August 9, 2022

Version of record online: August 31, 2022